Les Cahiers du GERAD ISSN: 0711–2440

Fleet and infrastructure planning for heavy-duty electric vehicles with opportunity charging

L. Wu, J. E. Mendoza, Y. Adulyasak, J.-F. Cordeau

G–2026–38

July 2026

Citation suggérée : L. Wu, J. E. Mendoza, Y. Adulyasak, J.-F. Cordeau (Juillet 2026). Fleet and infrastructure planning for heavy-duty electric vehicles with opportunity charging, Rapport technique, Les Cahiers du GERAD G– 2026–38, GERAD, HEC Montréal, Canada.

Avant de citer ce rapport technique, veuillez visiter notre site Web (https://www.gerad.ca/fr/papers/G-2026-38) afin de mettre à jour vos données de référence, s'il a été publié dans une revue scientifique.

Suggested citation: L. Wu, J. E. Mendoza, Y. Adulyasak, J.-F. Cordeau (July 2026). Fleet and infrastructure planning for heavy-duty electric vehicles with opportunity charging, Technical report, Les Cahiers du GERAD G–2026–38, GERAD, HEC Montréal, Canada.

Before citing this technical report, please visit our website (https://www.gerad.ca/en/papers/G-2026-38) to update your reference data, if it has been published in a scientific journal.

La publication de ces rapports de recherche est rendue possible grâce au soutien de HEC Montréal, Polytechnique Montréal, Université McGill, Université du Québec à Montréal, ainsi que du Fonds de recherche du Québec – Nature et technologies.

Dépôt légal – Bibliothèque et Archives nationales du Québec, 2026
– Bibliothèque et Archives Canada, 2026

The publication of these research reports is made possible thanks to the support of HEC Montréal, Polytechnique Montréal, McGill University, Université du Québec à Montréal, as well as the Fonds de recherche du Québec – Nature et technologies.

Legal deposit – Bibliothèque et Archives nationales du Québec, 2026
– Library and Archives Canada, 2026

GERAD HEC Montréal
3000, chemin de la Côte-Sainte-Catherine
Montréal (Québec) Canada H3T 2A7

Tél. : 514 340-6053
Téléc. : 514 340-5665
info@gerad.ca
www.gerad.ca

Fleet and infrastructure planning for heavy-duty electric vehicles with opportunity charging

Lingxiao Wu [a]

Jorge E. Mendoza [b]

Yossiri Adulyasak [b, c]

Jean-François Cordeau [b, c]

[a] *Department of Aeronautical and Aviation Engineering, The Hong Kong Polytechnic University, Kowloon, Hong Kong*

[b] *Department of Logistics and Operations Management, HEC Montréal, Montréal (Qc), Canada, H3T 2A7*

[c] *GERAD, Montréal (Qc), Canada, H3T 1J4*

lingxiao-leo.wu@polyu.edu.hk
jorge.mendoza@hec.ca
yossiri.adulyasak@hec.ca
jean-francois.cordeau@hec.ca

July 2026
Les Cahiers du GERAD
G–2026–38

Abstract : Heavy-duty vehicles (HDVs) are a major source of road transportation emissions, yet their electrification remains challenging due to operational constraints. Opportunity charging, which enables electric vehicles to recharge without interrupting regular operations, offers a practical solution for electrifying certain HDV sectors. Motivated by a real-world electrification planning problem in seaport container drayage, this paper addresses the large-scale electrification planning problem for HDV fleets through opportunity charging, optimizing both fleet composition and charging infrastructure deployment. We formulate the problem as a mixed-integer linear program and propose an exact solution algorithm based on Benders decomposition. The algorithm splits the problem into a master problem for fleet composition and charging infrastructure deployment and a large number of subproblems for en-route charging scheduling. In view of the computational burden from solving the master and subproblems, we develop novel acceleration strategies, including problem-specific valid inequalities and subproblem reduction techniques. The algorithm was tested using instances generated from data of a real-world electrification project. The results demonstrate that the strategies significantly improve the performance of the algorithm and that our approach solves realistic-scale instances (e.g., 50 vehicles and over 50 candidate charging stations) to near-optimality within practical computational times. The results also reveal that opportunity charging can achieve cost reductions of over 30% and emissions reductions of up to 94% compared to conventional fleets, while maintaining operational feasibility.

Keywords : Electric vehicles; opportunity charging; fleet composition; charging facility location; Benders decomposition

1 Introduction

Road transportation accounts for approximately 10% of global anthropogenic carbon emissions (Nemet et al. 2022). Electrification is widely regarded as a promising pathway to decarbonize this sector. According to the studies of International Energy Agency (2024), electric vehicles (EVs) have 50% lower life-cycle emissions than internal combustion engine vehicles (ICEVs). From an economic perspective, EVs are increasingly competitive with ICEVs. For instance, in Canada, energy costs for medium-sized EVs are $3-4$ Canadian cents per kilometer (km), compared to $11-12$ Canadian cents for gasoline vehicles,[1] while purchase prices now rival ICEVs due to declining battery costs (International Energy Agency 2024). These environmental and economic benefits position EVs as a viable alternative to ICEVs.

However, the adoption of EVs faces significant challenges, including limited driving range, lengthy recharging times, and insufficient recharging infrastructure. Recent advancements in battery technology

and the expansion of charging infrastructure are beginning to mitigate these issues, particularly for light-duty vehicles (e.g., passenger cars). Currently, electric passenger cars can travel between 360 and 380 km on a single charge and can be recharged in about 10 hours using standard chargers, or in under an hour with fast chargers.[2] By recharging overnight at depots, light-duty EVs are increasingly able to match the performance of ICEVs in many scenarios.

The situation for electric heavy-duty vehicles (HDVs), such as buses and trucks, is more complex. For instance, an electric heavy-duty truck capable of an 800 km journey requires a battery weighing at least 5,500 kilograms and approximately 20 hours to recharge (Cunanan et al. 2021). Given the long operational hours of most commercial HDVs, extended recharging times can be economically burdensome. Therefore, despite the substantial environmental benefits and energy cost savings, the heavy batteries and long charging times significantly impede the progress of HDV electrification. In 2023, while EVs constituted 18% of light-duty vehicle sales, they constituted just 3% of HDV sales (International Energy Agency 2024).

Opportunity charging, which leverages fast charging technologies, offers a potential solution to some of these challenges by allowing EVs to utilize lighter batteries and recharge without interrupting regular operations. Recent improvements in autonomous wireless power transfer techniques (Alabsi et al. 2024) and supercapacitors (Horn et al. 2019) have further enhanced the viability of opportunity charging. Notably, supercapacitors are capable of storing and releasing energy much more quickly than Li-ion batteries (Horn et al. 2019), although they have a much more limited energy capacity. With these advancements, wireless charging systems can achieve transfer speeds as high as 500 kW.[3] Wireless charging systems have been adopted by various HDV electrification projects, covering cargo drayage, bus transit, and regional deliveries. Additionally, to prevent energy depletion, hybrid HDVs are a viable option for the electrification of HDVs, especially those in Class-8 (i.e., with the heaviest duties) (Zhao et al. 2013, Moghadasi et al. 2024).

Figure 1 illustrates examples of opportunity charging for heavy-duty EVs. Although not all heavy-duty transportation sectors are amenable to opportunity charging, operations with predictable routes and regular stops, such as bus services, urban and regional delivery services, and drayage operations at cargo terminals, are ideal candidates. For instance, fast opportunity charging enables 24/7 bus services in Kent County Council, the UK, maintaining schedules without the need for return-to-depot charging.[4] The studies by Estrada et al. (2022) and Vendé et al. (2025) have also demonstrated the environmental and economic benefits of opportunity charging for EVs and hybrid EVs in urban

[1] Source: https://natural-resources.canada.ca/energy-efficiency/transportation-alternative-fuels/personal-vehicles/choosing-right-vehicle/buying-electric-vehicle/21034.

[2] Source: https://www.transportation.gov/rural/ev/toolkit/ev-basics/charging-speeds.

[3] Source: https://www.ajot.com/news/deployment-of-500kw-inductive-charger-to-power-electric-trucks-in-cold-climates/.

[4] Source: https://www.vev.com/blog/opportunity-charging-for-ev-buses-pantograph-technology/.

bus services. On top of these examples, the Government of Canada also estimated that deploying fast opportunity chargers at destination locations will also play a critical role in the electrification of HDV fleets, especially in early market development stages. Additionally, it noted that the widespread deployment of opportunity chargers across the country is essential in the near future.[5]

(a) (b)

Figure 1: Samples of opportunity charging for HDVs: (a) Bus services, (b) Container drayage (Crawford 2020, Morris 2022, Li et al. 2023, InsideEVs 2022).

To electrify a fleet of vehicles with opportunity charging requires solving a complex problem that involves three interconnected decisions: (i) the configurations of the EV fleet, (ii) the locations of the opportunity charging facilities, and (iii) the charging schedules of the EVs. This paper addresses the electrification planning problem with opportunity charging (EPPOC) faced by HDV operators. Our study makes the following main contributions:

First, given the globally rising demand for HDV electrification and inspired by a real-world electrification project from our industrial partner, we introduce the EPPOC for HDV operations. This problem jointly optimizes fleet renewal, charging facility deployment, and vehicle charging scheduling. We formulate the problem as a compact mixed-integer linear programming (MILP) model.

Second, an exact solution algorithm is developed based on Benders decomposition. Within the solution framework, a polynomial-time solution algorithm is designed for the subproblems where the dwelling time of vehicles at each location is fixed. Additionally, to alleviate the computational burden from a large number of subproblems in the decomposition, we propose a series of acceleration strategies, including a novel subproblem reduction method. We demonstrate that the number of subproblems solved in Benders decomposition can be significantly reduced while the convergence of the algorithm is still ensured. The framework of the algorithm and its enhancement strategies are sufficiently general and can be adapted to similar planning optimization problems that involve a two-level "deployment-then-evaluation" structure.

Third, we conduct extensive numerical experiments using data instances generated from a real electrification project for drayage operations at a major container terminal. The results demonstrate that our solution approach can obtain optimal or near-optimal solutions within reasonable computational times. Furthermore, our results reveal that opportunity charging reduces total costs by over 30% and cuts emissions by up to 94% compared to conventional HDV fleets. This demonstrates a Pareto-efficient pathway to decarbonize road freight without sacrificing economic viability.

The remainder of this paper is structured as follows. We review the relevant studies in Section 2. We formally describe the problem and formulate it as a compact MILP model in Section 3. We describe the Benders reformulation of the model in Section 4. In Section 5, we propose several enhancement strategies to the basic Benders decomposition algorithm. We report computational experiments in Section 6, followed by conclusions in Section 7. We provide all mathematical proofs in EC.2 of the electronic companion.

[5]Source: https://natural-resources.canada.ca/energy-efficiency/transportation-energy-efficiency/resource-library/electric-vehicle-charging-infrastructure-canada.

2 Literature review

Operations management problems associated with EV operations have garnered significant attention in recent years (Perumal et al. 2022). Our study closely aligns with three specific areas within EV operations: the fleet renewal problem, the charging facility deployment problem, and the en-route opportunity charging scheduling problem. The first two are strategic planning problems, whereas the third one pertains to operational-level decisions.

At the strategic level, the planning problems related to both fleet renewal and charging facility deployment have been extensively studied in the literature. Ansaripoor et al. (2016) investigated a fleet replacement problem that helps organizations determine bus replacement plans to meet their carbon footprint reduction targets in a cost-effective manner. Similar problems have been considered in the context of trucking companies (Bakır 2017), taxi companies (La Rocca and Cordeau 2019), transit bus service providers (Pelletier et al. 2019), and carsharing service operators (Xu et al. 2018). The charging facility deployment problem focuses on strategically placing charging facilities within a transportation network. The main objective of this problem is to maximize the traffic flow volume that can be recharged, respecting the range limitations of the vehicles (Arslan and Karaşan 2016). Studies on the deployment of opportunity chargers are primarily focused on the context of electric bus services (e.g., Liu et al. 2018, Vendé et al. 2025). In particular, Vendé et al. (2025) investigated a problem of optimizing the deployment of opportunity chargers in a hybrid electric bus network with the objective of maximizing the total distance driven using the electric mode. They proposed a MILP model and developed a branch-and-check solution algorithm for the problem.

At the operational level, the en-route opportunity charging scheduling problem is concerned with deciding the charging time of a vehicle at each charging facility on a given road. He et al. (2020) considered a charging scheduling problem on a bus network with changeable electricity rates. The problem was reformulated as a linear programming (LP) model. Abdelwahed et al. (2020) proposed two MILP models for optimizing the charging schedules of buses at opportunity charging stations on a bus network. The result demonstrated that opportunity charging is critical in extending the service range of buses. The en-route charging scheduling problem has also been considered in some studies as a subproblem in the EV routing problem, formulated based on a given route of an EV (Kullman et al. 2021, Yamín et al. 2025).

Since these problems are interconnected, some studies handled them in an integrated manner. Most of such studies focused on the integrated charging station location and en-route charging problem (e.g., Li et al. 2024). The integration of all three problems has also been investigated in some studies on the electrification of transit bus services (Alwesabi et al. 2021, Gairola and Nezamuddin 2023, He et al. 2023, Zhang et al. 2025), and solution algorithms based on Lagrangian relaxation (An 2020) and metaheuristics (Ko and Jang 2013) have been developed.

Concluding, problems related to the operations management of EVs have been the object of considerable research and the integration of the three problems discussed above, similar to the EPPOC, has been considered in the literature. However, the integrated optimization problems studied in the literature have either been applied to relatively small instances that allow for the direct application of solvers (i.e., those involving single or several bus lines) (Alwesabi et al. 2021, Gairola and Nezamuddin 2023) or rely on heuristic algorithms for constructing feasible solutions to large-scale instances (An 2020, Ko and Jang 2013). In contrast, this study develops exact solution algorithms for this challenging problem.

3 Problem statement and compact formulation

In the EPPOC, we are given a set of diesel-fueled vehicles, each operating on a set of routes in a network. Depending on the application context, these routes correspond to bus trips in urban transit services, haulage paths in freight transportation, trips in urban or regional delivery, or trucking paths in terminal drayage.

The problem involves decision-making at both strategic and operational levels. At the strategic level, decisions relate to vehicle retrofit and charging station deployment. At the operational level, in response to the strategic decisions, given a route of each vehicle, the optimal en-route charging schedule is determined. The objective of the problem is to find an electrification strategy and a set of charging schedules such that the expected total operating cost is minimized.

Globally, startups and legacy automakers are developing solutions to implement opportunity charging in new trucks or retrofit existing fleets. For example, Montréal-based Effenco retrofits heavy-duty diesel trucks with an electric propulsion motor, ultracapacitor energy storage, a wireless inductive charging system, and a diesel range extender.[6] Our problem definition builds upon this technological approach. Sections 3.1 and 3.2 model the strategic electrification decisions and the en-route charging schedules, respectively. The full formulation is given in Section 3.3.

For notational clarity throughout this paper, we define the following notation: given any positive integer N, the set $[N]$ denotes all non-negative integers up to N, i.e., $[N] = \{0, ..., N\}$, while $[N]^+$ denotes the set of all positive integers up to N, i.e., $[N]^+ = \{1, ..., N\}$. The cardinality of any set $\mathcal{A}$ is denoted by $|\mathcal{A}|$. Additionally, vector quantities are represented in boldface lowercase letters. We summarize the notation used in the formulation in EC.1 of the electronic companion.

3.1 Strategic electrification decisions

We consider a fleet comprised of F homogeneous diesel-fueled vehicles and a set $\mathcal{H}$ of potential configurations for their electrification. For each configuration $h \in \mathcal{H}$, there are associated parameters: a default charging rate p_h, a battery capacity q_h, and a cost of retrofitting C^1_h. Once retrofitted, a diesel vehicle becomes a hybrid one, which is primarily powered by electricity and switches to the diesel model automatically after depleting its battery.

The operations of these vehicles are modeled on a directed network $\mathcal{G} = (\mathcal{V}, \mathcal{E})$, with $\mathcal{V}$ representing the vertices (locations) and $\mathcal{E}$ the edges (paths between locations). Let $\mathcal{V}' \subseteq \mathcal{V}$ be the set of candidate sites for the deployment of charging stations. The set of charging station types is denoted by $\mathcal{K}$. Each station type $k \in \mathcal{K}$ has a distinct charging rate g_k and an associated construction cost $C^2_{v,k}$ for a given vertex $v \in \mathcal{V}'$. The fleet operator is allocated a budget denoted by B for fleet retrofitting and charging station deployment.

We consider a single-period decision problem, where all strategic decisions are made once at the beginning and remain fixed for the entire planning horizon. The electrification decisions are represented by two sets of binary variables. In particular, the retrofit decisions are denoted by $x_{f,h}$, which is set to 1 if, and only if, $f \in [F]$ vehicles in the fleet are retrofitted with the electrification configuration $h \in \mathcal{H}$. Additionally, for the deployment of charging facilities, we let $y_{v,k}$ equal 1 if, and only if, a charging station of type $k \in \mathcal{K}$ is deployed at vertex $v \in \mathcal{V}$.

The constraints for the electrification decisions are given in the electrification set denoted by $\mathbf{X}$, which is defined as follows:

$$\mathbf{X} = \{\boldsymbol{x}, \boldsymbol{y} | (1) - (6)\},$$

where

$$\sum_{f \in [F]} \sum_{h \in \mathcal{H}} f x_{f,h} = F, \tag{1}$$

$$\sum_{k \in \mathcal{K}} y_{k,v} \leq 1 \qquad \forall v \in \mathcal{V}, \tag{2}$$

[6]Illustrations of Effenco's products: https://www.effenco.com/100-electric/.

$$\sum_{k \in \mathcal{K}} y_{k,v} = 0 \qquad \forall v \in \mathcal{V} \setminus \mathcal{V}', \tag{3}$$

$$\sum_{f \in [F]} \sum_{h \in \mathcal{H}} C_h^1 f x_{f,h} + \sum_{k \in \mathcal{K}} \sum_{v \in \mathcal{V}} C_{v,k}^2 y_{v,k} \leq B, \tag{4}$$

$$x_{f,h} \in \{0,1\} \qquad \forall f \in [F], h \in \mathcal{H}, \tag{5}$$

$$y_{v,k} \in \{0,1\} \qquad \forall k \in \mathcal{K}, v \in \mathcal{V}. \tag{6}$$

Constraint (1) ensures that each vehicle is retrofitted with exactly one configuration. Constraints (2) and (3) require that each vertex can install at most one charging station and that charging stations can only be built on eligible vertices, respectively. Constraint (4) sets the upper limit for investments in electrification, indicating the maximum cost that the operator can afford for the electrification project. The domains of decision variables in $\boldsymbol{x}$ and $\boldsymbol{y}$ are given by constraints (5) and (6).

3.2 En-route charging scheduling

The operations of the fleet in a certain period (e.g., a day or a work shift) can be represented as a set of *routes* on the network $\mathcal{G}$. Let $\mathcal{R}$ denote the set of routes we use to assess the impact of electrification decisions. If the vehicles are operated on fixed service routes in the EPPOC (e.g., the problem associated with bus services), then one can construct $\mathcal{R}$ based on the real bus routes. Meanwhile, for the case where vehicles are operated on demand (e.g., the EPPOC associated with delivery services or drayage), then $\mathcal{R}$ can be generated by sampling from historical service routes of the vehicles.

Each route originates and ends at the (dummy) depot and traverses through a sequence of vertices in $\mathcal{V}$. A route $r \in \mathcal{R}$ comprises a set of legs $\mathcal{L}_r$, each representing a journey segment, either for passenger or freight movement (loaded trip) or vehicle repositioning (empty trip). Let $\mathcal{L} = \bigcup_{r \in \mathcal{R}} \mathcal{L}_r$ denote the full set of legs from all routes. Each leg $l \in \mathcal{L}$ consists of a set of sequenced *nodes*, including a start node, an end node, and a series of intermediary nodes forming the shortest path between them. We let $\mathcal{N}_l \subseteq \mathcal{N}$ denote the set of nodes within any leg $l \in \mathcal{L}$. For any node $i \in \mathcal{N}_l$, w_i defines the minimum dwell time of any vehicle on the node and represents the service time for passenger boarding/deboarding or cargo handling. In particular, we have $w_i \geq 0$ if i represents the start or end node of a leg with service demand and $w_i = 0$ if it represents an intermediary node without service demand. When traveling on a leg, vehicles are allowed to stay at a node longer than the required service time for recharging. To limit service delays, we set a maximum allowable total dwell time of any vehicle on the nodes of any leg $l \in \mathcal{L}$, which is denoted by T_l.

For each route $r \in \mathcal{R}$, given the nodes within each leg of the route, we let $\mathcal{N}_r$ be the set of sequenced nodes on that route. Let $N_r = |\mathcal{N}_r|$ be the count of nodes for route $r \in \mathcal{R}$, and we use $i(r,n) \in \mathcal{N}_r$ to represent the n-th node visited on route r, where $n \in [N_r]^+$ and $r \in \mathcal{R}$. Furthermore, the set of arcs contained in route r is denoted by $\mathcal{A}_r$, with $a(r,n)$ representing the n-th arc, where $n \in [N_r - 1]^+$. The length of arc $a \in \mathcal{A}_r$ is given by d_a, where $r \in \mathcal{R}$. Additionally, we use $\mathcal{N} = \bigcup_{r \in \mathcal{R}} \mathcal{N}_r$ and $\mathcal{A} = \bigcup_{r \in \mathcal{R}} \mathcal{A}_r$ to represent the full set of nodes and arcs covering all routes. Furthermore, the physical (non-sequenced) vertex on the network $\mathcal{G}$ corresponding to node $i \in \mathcal{N}$ is denoted by $v(i) \in \mathcal{V}$.

As for the operations of the vehicles, when running on the routes, a vehicle equipped with configuration $h \in \mathcal{H}$ consumes b units of electricity for each unit of distance traveled under electric power. The initial battery charge for a vehicle with any configuration $h \in \mathcal{H}$ embarking on a route is denoted by α_h^0.

Finally, we introduce decision variables for modeling the charging schedule of any vehicle along route $r \in \mathcal{R}$. Given any vehicle with configuration $h \in \mathcal{H}$, we let $u_{h,i}$ reflect the dwelling time at node $i \in \mathcal{N}_r$. The remaining battery charge upon arrival at node $i \in \mathcal{N}_r$ and the electricity recharged at the node are denoted by $\alpha_{h,i}$ and $\beta_{h,i}$, respectively. Furthermore, for each arc $a \in \mathcal{A}$, $\mu_{h,a}$ and $\nu_{h,a}$ represent the distances traversed in electric and diesel modes by the vehicle, respectively.

The following constraints are used to regulate the en-route charging procedure of vehicles:

$$u_{h,i} \geq w_i \qquad \forall i \in \mathcal{N}, h \in \mathcal{H}, \tag{7}$$

$$\sum_{i \in \mathcal{N}_l} u_{h,i} \leq T_l \qquad \forall l \in \mathcal{L}, h \in \mathcal{H}, \tag{8}$$

$$\mu_{h,a} + \nu_{h,a} = d_a \qquad \forall a \in \mathcal{A}, \tag{9}$$

$$\alpha_{h,i(r,1)} = \alpha_h^0 \qquad \forall r \in \mathcal{R}, h \in \mathcal{H}, \tag{10}$$

$$\alpha_{h,i} + \beta_{h,i} \leq q_h \qquad \forall i \in \mathcal{N}, h \in \mathcal{H}, \tag{11}$$

$$\alpha_{h,i(r,n+1)} = \alpha_{h,i(r,n)} + \beta_{h,i(r,n)} - b\mu_{h,a(r,n)} \qquad \forall r \in \mathcal{R}, n \in [N_r - 1]^+, h \in \mathcal{H}, \tag{12}$$

$$\beta_{h,i} \leq u_{h,i} \sum_{k \in \mathcal{K}} g_k y_{k,v(i)} \qquad \forall i \in \mathcal{N}, h \in \mathcal{H}, \tag{13}$$

$$\beta_{h,i} \leq p_h u_{h,i} \qquad \forall i \in \mathcal{N}, h \in \mathcal{H}, \tag{14}$$

$$u_{h,i}, \alpha_{h,i}, \beta_{h,i} \geq 0 \qquad \forall i \in \mathcal{N}, h \in \mathcal{H}, \tag{15}$$

$$\mu_{h,a}, \nu_{h,a} \geq 0 \qquad \forall a \in \mathcal{A}, h \in \mathcal{H}. \tag{16}$$

Constraints (7) secure sufficient service time at each node. Constraints (8) set the upper bound for the total dwelling time of a vehicle on each leg. Constraints (9) ensure that the sum of distances traveled by a vehicle in electric mode and diesel mode on an arc equals its distance. Constraints (10) require that each vehicle start its route with the initial battery charge. Constraints (11) ensure that the electricity stored on any vehicle is kept under the capacity of its selected configuration. Constraints (12) track the energy on a vehicle along a route. Constraints (13) and (14) set limits on the amount of electricity recharged on each node by each vehicle. They indicate that the charging rate for any vehicle at any vertex is determined by the lower value between the vehicle's configuration charging rate and the charging speed of the charging station at that vertex, if available. That is, we have $\beta_{h,i} \leq u_{h,i} \sum_{k \in \mathcal{K}} \min\{g_k, p_h\} y_{k,v(i)}$, $\forall i \in \mathcal{N}, h \in \mathcal{H}, i \in \mathcal{N}, h \in \mathcal{H}$. Finally, constraints (15) and (16) impose that the decision variables should be non-negative.

Note that the quadratic constraints (13) can be linearized through the following constraints:

$$\gamma_{h,k,i} \leq g_k u_{h,i} \qquad \forall i \in \mathcal{N}, k \in \mathcal{K}, h \in \mathcal{H}, \tag{17}$$

$$\gamma_{h,k,i} \leq M^1_{h,k,i} y_{k,v(i)} \qquad \forall i \in \mathcal{N}, k \in \mathcal{K}, h \in \mathcal{H}, \tag{18}$$

$$\beta_{h,i} \leq \sum_{k \in \mathcal{K}} \gamma_{h,k,i} \qquad \forall i \in \mathcal{N}, h \in \mathcal{H}, \tag{19}$$

$$\gamma_{h,k,i} \geq 0 \qquad \forall i \in \mathcal{N}, k \in \mathcal{K}, h \in \mathcal{H}, \tag{20}$$

where $M^1_{h,k,i} = \max\left\{\min\{g_k \bar{t}_i, p_h \bar{t}_i, q_h\}, 0\right\}$ gives the upper limits for the amount of electricity that can be recharged, at node $i \in \mathcal{N}$, given the type of the charging station $k \in \mathcal{K}$ and vehicle configuration $h \in \mathcal{H}$. Here $\bar{t}_i = T_l - \sum_{j \in \mathcal{N}_l \setminus \{i\}} \{s_j\}$ represents the maximum recharging time at node $i \in \mathcal{N}_l$ on leg $l \in \mathcal{L}$.

3.3 Full formulation

The objective of the EPPOC is to formulate an electrification plan that minimizes the expected total cost in a planning horizon. Before presenting the full formulation, we introduce the following additional notation. Let D and E denote the unit-distance cost of any vehicle for energy consumption under the diesel and electric modes, respectively. It is assumed that $D > E$, which indicates that vehicles have lower unit-distance cost when running in electric mode than diesel mode. Note that these costs can include not only the price of the energy, but also carbon taxes or credits. Let also o_r represent the weight of route $r \in \mathcal{R}$ for calculating its contribution in the expected total cost within the planning horizon for electrification. In practice, o_r may reflect factors such as the frequency of a route (e.g., in transit services) or managerial preferences. In addition, we introduce variable $z_{h,r}$, which represents the energy consumption cost of any vehicle with configuration $h \in \mathcal{H}$ running on route $r \in \mathcal{R}$. Finally, let Z denote the expected operational costs for running the entire fleet during the planning horizon. The full formulation of the problem is given as follows:

$$\min \quad \sum_{f\in[F]^+}\sum_{h\in\mathcal{H}} C_h^1 f x_{f,h} + \sum_{k\in\mathcal{K}}\sum_{v\in\mathcal{V}^1} C_{k,v}^2 y_{k,v} + Z \tag{21a}$$

$$\text{s.t.} \qquad (1)-(12), (14)-(20), \text{ and,}$$

$$z_{h,r} = E\sum_{a\in\mathcal{A}_r}\mu_{h,a} + D\sum_{a\in\mathcal{A}_r}\nu_{h,a} \qquad \forall r\in\mathcal{R}, h\in\mathcal{H}, \tag{21b}$$

$$Z = \sum_{f\in[F]^+}\sum_{r\in\mathcal{R}}\sum_{h\in\mathcal{H}} o_r f x_{f,h} z_{h,r}. \tag{21c}$$

The objective function (21a) minimizes the expected total cost, which includes three components. The first and second terms are the costs for electrifying the fleet and setting up charging stations, respectively. The third term is the total expected operational costs for running the fleet during the planning horizon. Constraints (21b) calculate the cost of a vehicle with any configuration $h \in \mathcal{H}$ for running on any route $r \in \mathcal{R}$. Finally, Z is calculated through constraints (21c). We linearize the quadratic equation (21c) for calculating Z as follows:

$$Z = \sum_{f\in[F]^+}\sum_{h\in\mathcal{H}} f\phi_{f,h}, \tag{22}$$

$$\phi_{f,h} \geq \sum_{r\in\mathcal{R}} o_r z_{h,r} + M^2(x_{f,h}-1) \qquad \forall f\in[F]^+, h\in\mathcal{H}, \tag{23}$$

$$\phi_{f,h} \geq 0 \qquad \forall f\in[F]^+, h\in\mathcal{H}, \tag{24}$$

where $M^2 = \sum_{r\in\mathcal{R}} o_r D \sum_{a\in\mathcal{A}_r} d_a$ gives the upper bound of the expected total operational cost of any vehicle in the planning horizon.

The formulation can be strengthened by eliminating symmetry issues that stem from the homogeneity of the original diesel fleet. In particular, for all the $x_{f,h}$ variables associated with the same h, we use the following symmetry-breaking constraints to allow at most one variable to be equal to 1:

$$\sum_{f\in[F]} x_{f,h} = 1, \qquad \forall h\in\mathcal{H}. \tag{25}$$

The model with objective function (21a) and constraints (1)–(12), (14)–(20), (21b), and (22)–(25) is referred to as M1. Note that M1 is a MILP model. While the model can be solved with off-the-shelf optimization solvers, their capability is limited only to instances with small scale. To solve instances with realistic scale, we introduce a tailored Benders decomposition solution approach in the following section.

4 Benders reformulation

We observe that in the EPPOC, once the strategic electrification decisions (i.e., the $\boldsymbol{x}$ and $\boldsymbol{y}$ variables) are fixed, the remaining problem reduces to an en-route charging problem which can be further decomposed by routes and vehicle configurations. This leads to a decomposition framework where the master problem addresses the strategic electrification decisions and each subproblem solves the en-route charging scheduling problem for a specific route $r \in \mathcal{R}$ and vehicle configuration $h \in \mathcal{H}$.

Given any solution $(\bar{\boldsymbol{x}}, \bar{\boldsymbol{y}}) \in \mathbf{X}$, the primal en-route charging scheduling subproblem associated with route $r \in \mathcal{R}$ and vehicle configuration $h \in \mathcal{H}$, denoted by $\text{PSP}_{h,r}(\bar{\boldsymbol{x}}, \bar{\boldsymbol{y}})$, can be formulated as follows:

$$\min_{[\text{PSP}_{h,r}(\bar{\boldsymbol{x}},\bar{\boldsymbol{y}})]} \quad E\sum_{a\in\mathcal{A}_r}\mu_{h,a} + D\sum_{a\in\mathcal{A}_r}\nu_{h,a} \tag{26a}$$

$$
\begin{aligned}
\text{s.t.} \quad & u_{h,i} \geq w_i && \forall i \in \mathcal{N}_r, && (26b)\\
& \sum_{i \in \mathcal{N}_l} u_{h,i} \leq T_l && \forall l \in \mathcal{L}_r, && (26c)\\
& \mu_{h,a} + \nu_{h,a} = d_a && \forall a \in \mathcal{A}_r, && (26d)\\
& \alpha_{h,i(r,1)} = \alpha_h^0, && && (26e)\\
& \alpha_{h,i} + \beta_{h,i} \leq q_h && \forall i \in \mathcal{N}_r, && (26f)\\
& \alpha_{h,i(r,n+1)} = \alpha_{h,i(r,n)} + \beta_{h,i(r,n)} - b\mu_{h,a(r,n)} && \forall n \in [N_r - 1]^+, && (26g)\\
& \gamma_{h,k,i} \leq g_k u_{h,i} && \forall i \in \mathcal{N}_r, k \in \mathcal{K}, && (26h)\\
& \gamma_{h,k,i} \leq M^1_{h,k,i} \bar{y}_{k,v(i)} && \forall i \in \mathcal{N}_r, k \in \mathcal{K}, && (26i)\\
& \beta_{h,i} \leq \sum_{k \in \mathcal{K}} \gamma_{h,k,i} && \forall i \in \mathcal{N}_r, && (26j)\\
& \beta_{h,i} \leq p_h u_{h,i} && \forall i \in \mathcal{N}_r, && (26k)\\
& u_{h,i}, \alpha_{h,i}, \beta_{h,i}, \gamma_{h,k,i}, \mu_{h,a}, \nu_{h,a} \geq 0 && \forall a \in \mathcal{A}_r, i \in \mathcal{N}_r, k \in \mathcal{K}. && (26l)
\end{aligned}
$$

Let $\boldsymbol{\eta}_{h,r} = (\eta_i | i \in \mathcal{N}_r)$, $\boldsymbol{\theta}_{h,r} = (\theta_l | l \in \mathcal{L}_r)$, $\boldsymbol{\vartheta}_{h,r} = (\vartheta_a | a \in \mathcal{A}_r)$, $\boldsymbol{\kappa}_{h,r} = (\kappa)$, $\boldsymbol{\psi}_{h,r} = (\psi_i | i \in \mathcal{N}_r)$, $\boldsymbol{\pi}_{h,r} = (\pi_n | n \in [N_r - 1]^+)$, $\boldsymbol{\rho}_{h,r} = (\rho_{i,k} | i \in \mathcal{N}_r, k \in \mathcal{K})$, $\boldsymbol{\varrho}_{h,r} = (\varrho_{i,k} | i \in \mathcal{N}_r, k \in \mathcal{K})$, $\boldsymbol{\phi}_{h,r} = (\phi_i | i \in \mathcal{N}_r)$, and $\boldsymbol{\varphi}_{h,r} = (\varphi_i | i \in \mathcal{N}_r)$ denote the vectors of dual variables associated with constraints (26b)–(26k), respectively. For notational simplicity, let $\boldsymbol{\chi}_{h,r} := (\boldsymbol{\eta}_{h,r}, \boldsymbol{\theta}_{h,r}, \boldsymbol{\vartheta}_{h,r}, \boldsymbol{\kappa}_{h,r}, \boldsymbol{\psi}_{h,r}, \boldsymbol{\pi}_{h,r}, \boldsymbol{\rho}_{h,r}, \boldsymbol{\varrho}_{h,r}, \boldsymbol{\phi}_{h,r}, \boldsymbol{\varphi}_{h,r})$.

The dual of the primal problem $\text{PSP}_{h,r}(\bar{\boldsymbol{x}}, \bar{\boldsymbol{y}})$, denoted by $\text{DSP}_{h,r}(\bar{\boldsymbol{x}}, \bar{\boldsymbol{y}})$, can be formulated as follows:

$$
\begin{aligned}
\underset{[\text{DSP}_{h,r}(\bar{\boldsymbol{x}}, \bar{\boldsymbol{y}})]}{\min} \quad & \sum_{i \in \mathcal{N}_r} w_i \eta_i + \sum_{l \in \mathcal{L}_r} T_l \theta_l + \sum_{a \in \mathcal{A}_r} d_a \vartheta_a + \alpha_h^0 \kappa + \sum_{i \in \mathcal{N}_r} q_h \psi_i + \sum_{k \in \mathcal{K}} \sum_{i \in \mathcal{N}_r} M^1_{h,k,i} \bar{y}_{k,v(i)} \varrho_{i,k} && (27a)\\
\text{s.t.} \quad & \eta_i + \theta_l - \sum_{k \in \mathcal{K}} g_k \rho_{i,k} - p_h \varphi_i \leq 0 \quad \forall i \in \mathcal{N}_l, l \in \mathcal{L}_r, && (27b)\\
& \vartheta_{a(r,n)} + b\pi_n \leq E \quad \forall n \in [N_r - 1]^+, && (27c)\\
& \vartheta_{a(r,n)} \leq D \quad \forall n \in [N_r - 1]^+, && (27d)\\
& \kappa + \psi_{i(r,1)} - \pi_1 \leq 0, && (27e)\\
& \psi_{i(r,n)} + \pi_{n-1} - \pi_n \leq 0 \quad \forall n \in [N_r - 1]^+ : n \neq 1, && (27f)\\
& \psi_{i(r,N_r)} + \pi_{N_r - 1} \leq 0, && (27g)\\
& \psi_{i(r,n)} - \pi_n + \phi_{i(r,n)} + \varphi_{i(r,n)} \leq 0 \quad \forall n \in [N_r - 1]^+, && (27h)\\
& \psi_{i(r,N_r)} + \phi_{i(r,N_r)} + \varphi_{i(r,N_r)} \leq 0, && (27i)\\
& \rho_{i,k} + \varrho_{i,k} - \phi_i \leq 0 \quad \forall i \in \mathcal{N}_r, k \in \mathcal{K}, && (27j)\\
& \eta_i \geq 0 \quad \forall i \in \mathcal{N}_r, && (27k)\\
& \theta_l, \psi_i, \rho_{i,k}, \varrho_{i,k}, \phi_i, \varphi_i \leq 0 \quad \forall i \in \mathcal{N}_r, a \in \mathcal{A}_r, l \in \mathcal{L}_r, k \in \mathcal{K}. && (27l)
\end{aligned}
$$

Theorem 1. The primal and dual subproblems $\text{PSP}_{h,r}(\bar{\boldsymbol{x}}, \bar{\boldsymbol{y}})$ and $\text{DSP}_{h,r}(\bar{\boldsymbol{x}}, \bar{\boldsymbol{y}})$ are feasible and bounded, for any $(\bar{\boldsymbol{x}}, \bar{\boldsymbol{y}}) \in \mathbf{X}$, $h \in \mathcal{H}$, and $r \in \mathcal{R}$.

Theorem 1 indicates that only Benders optimality cuts are needed for formulating the master problem in the reformulation. While solving the dual subproblems $\text{DSP}_{h,r}(\bar{\boldsymbol{x}}, \bar{\boldsymbol{y}})$ generally requires calling an LP solver, Proposition 1 indicates that there exists an efficient exact algorithm that solves any $\text{DSP}_{h,r}(\bar{\boldsymbol{x}}, \bar{\boldsymbol{y}})$ such that $\sum_{i \in \mathcal{N}_l} w_i = T_l$, $\forall l \in \mathcal{L}_r$ in $\mathcal{O}(|\mathcal{N}_r||\mathcal{K}|)$ time.

Proposition 1. There exists an exact algorithm that solves any $\text{DSP}_{h,r}(\bar{\boldsymbol{x}}, \bar{\boldsymbol{y}})$ such that $\sum_{i \in \mathcal{N}_l} w_i = T_l$, $\forall l \in \mathcal{L}_r$ in $\mathcal{O}(|\mathcal{N}_r||\mathcal{K}|)$ time, where $h \in \mathcal{H}$, $r \in \mathcal{R}$, and $(\bar{\boldsymbol{x}}, \bar{\boldsymbol{y}}) \in \mathbf{X}$.

To define the optimality cuts, we let $\Lambda_{h,r}$ denote the polyhedrons defined by the constraints of problems $\text{DSP}_{h,r}(\bar{\boldsymbol{x}}, \bar{\boldsymbol{y}})$, for any $h \in \mathcal{H}$, $r \in \mathcal{R}$, and $(\bar{\boldsymbol{x}}, \bar{\boldsymbol{y}}) \in \mathbf{X}$. Note that $\Lambda_{h,r}$ is independent of $(\bar{\boldsymbol{x}}, \bar{\boldsymbol{y}})$. Let also $\mathbf{P}(\Lambda_{h,r})$ represent the set of extreme points of $\Lambda_{h,r}$, $\forall r \in \mathcal{R}, h \in \mathcal{H}$. We can then formulate the Benders master problem (MP) as follows:

$$\min_{[MP]} \quad \sum_{f\in[F]^+}\sum_{h\in\mathcal{H}} C_h^1 f x_{f,h} + \sum_{k\in\mathcal{K}}\sum_{v\in\mathcal{V}^1} C_{k,v}^2 y_{k,v} + Z \tag{28a}$$

$$\text{s.t.} \quad (1)-(6),(22)-(25), \text{ and,}$$

$$z_{h,r} \geq \sum_{i\in\mathcal{N}_r} w_i\eta_i + \sum_{l\in\mathcal{L}_r} T_l\theta_l + \sum_{a\in\mathcal{A}_r} d_a\vartheta_a + \alpha_h^0\kappa + \sum_{i\in\mathcal{N}_r} q_h\psi_i + \sum_{k\in\mathcal{K}}\sum_{i\in\mathcal{N}_r} M_{h,k,i}^1 \varrho_{i,k} y_{k,v(i)},$$
$$\forall\, \boldsymbol{\chi}_{h,r} \in \mathbf{P}(\Lambda_{h,r}), h\in\mathcal{H}, r\in\mathcal{R}. \tag{28b}$$

The MP contains an exponential number of Benders cuts (28b). Therefore, we design a solution algorithm that solves the MP in a cutting-plane manner. The algorithm starts from a relaxed MP where (28b) are dropped. It then detects violated Benders cuts by solving the dual subproblems and adds these cuts into the MP. The algorithm iterates between the master problem and the subproblems until no further violated Benders cuts can be separated. Details of the algorithm are elaborated in EC.3.1 of the electronic companion.

5 Computational enhancements

The efficiency of the Benders decomposition algorithm depends mainly on: (i) the number of iterations for the algorithm to converge, (ii) the computational effort required to solve the dual subproblems in each iteration, and (iii) the computational effort required to solve the MP in each iteration. In this section, we describe strategies that enhance the algorithm in these three aspects.

5.1 Pareto-optimal cuts

The convergence of a Benders decomposition algorithm can be impaired by the degeneracy of the primal subproblems, which leads to the presence of multiple optimal solutions to the dual subproblem. A common method to resolve this issue is to generate strong Benders cuts. Our approach adopts the technique suggested by Magnanti and Wong (1981) to produce high-quality, Pareto-optimal cuts.

To generate Pareto-optimal cuts, let $(\boldsymbol{x}^c, \boldsymbol{y}^c)$ denote a *core point* of the polyhedron associated with the LP relaxation of $\mathbf{X}$. Let also $\zeta_{h,r}$ denote the optimal objective function value to the dual subproblem $\mathrm{DSP}_{h,r}(\bar{\boldsymbol{x}}, \bar{\boldsymbol{y}})$, for any $h\in\mathcal{H}$, $r\in\mathcal{R}$, and $(\bar{\boldsymbol{x}}, \bar{\boldsymbol{y}})\in\mathbf{X}$. To generate Pareto-optimal cuts, we solve the following Pareto-optimal dual subproblem:

$$\max_{[PO-DSP_{h,r}(\bar{\boldsymbol{x}},\bar{\boldsymbol{y}},\zeta_{h,r},\boldsymbol{x}^c,\boldsymbol{y}^c)]} \quad \sum_{i\in\mathcal{N}_r} w_i\eta_i + \sum_{l\in\mathcal{L}_r} T_l\theta_l + \sum_{a\in\mathcal{A}_r} d_a\vartheta_a + \alpha_h^0\kappa + \sum_{i\in\mathcal{N}_r} q_h\psi_i$$
$$\text{s.t.} \quad + \sum_{k\in\mathcal{K}}\sum_{i\in\mathcal{N}_r} M_{h,k,i}^1 y_{k,v(i)}^c \varrho_{i,k}, \tag{29a}$$

$$(27b)-(27l), \text{ and,}$$

$$\sum_{i\in\mathcal{N}_r} w_i\eta_i + \sum_{l\in\mathcal{L}_r} T_l\theta_l + \sum_{a\in\mathcal{A}_r} d_a\vartheta_a + \alpha_h^0\kappa + \sum_{i\in\mathcal{N}_r} q_h\psi_i,$$
$$+ \sum_{k\in\mathcal{K}}\sum_{i\in\mathcal{N}_r} M_{h,k,i}^1 \varrho_{i,k}\bar{y}_{k,v(i)} = \zeta_{h,r}. \tag{29b}$$

5.2 Lower-bound lifting inequalities

Because parts of the objective function (21a) are projected out from the master problem in the Benders decomposition, the optimality gap in Benders decomposition can be large in the initial stages of the algorithm due to the low quality of the lower bound. A large number of iterations are thus needed before the convergence of the algorithm. To improve the lower bound, we propose to use lower-bound lifting (LBL) inequalities that contain some information about the parts in the objective function that are projected out. The following LBL inequalities are incorporated into the MP:

$$z_{h,r} \geq E \sum_{a\in\mathcal{A}_r} d_a \qquad \forall r \in \mathcal{R}, h \in \mathcal{H}, \tag{30}$$

$$z_{h,r} \geq D \sum_{a\in\mathcal{A}_r} d_a - (\alpha_h^0 + \sum_{i\in\mathcal{N}_r}\sum_{k\in\mathcal{K}} y_{k,v(i)} M^1_{h,k,i})/b(D-E), \qquad \forall r \in \mathcal{R}, h \in \mathcal{H}. \tag{31}$$

Observe that the right-hand-side of (30) computes the cost of running a vehicle on route $r \in \mathcal{R}$ entirely in electric mode, whereas the right-hand-side of (31) computes the cost of operating any vehicle with configuration $h \in \mathcal{H}$ on route $r \in \mathcal{R}$ under an optimistic estimation of the charged electricity. The following proposition formally proves their validity.

Proposition 2. Inequalities (30) and (31) are valid for the MP.

Consider a solution $(\bar{\boldsymbol{x}}, \bar{\boldsymbol{y}}) \in \mathbf{X}$ to the MP. Define $\mathcal{V}_r^1(\bar{\boldsymbol{y}})$ as the set of vertices along route $r \in \mathcal{R}$ with charging stations, represented by $\mathcal{V}_r^1(\bar{\boldsymbol{y}}) = \{v \in \mathcal{V} | \sum_{k\in\mathcal{K}} \bar{y}_{v,k} = 1, v(i) = v, \exists i \in \mathcal{N}_r\}$. Then, from Proposition 2, we have the following remark:

Remark 1. For any vehicle configuration $h \in \mathcal{H}$ and $r \in \mathcal{R}$, when $\mathcal{V}_r^1(\bar{\boldsymbol{y}}) = \varnothing$, (30) and (31) reduce to $z_{h,r} \geq \max\{D(\sum_{a\in\mathcal{A}_r} d_a - \alpha_h^0/b) + E(\alpha_h^0/b), E\sum_{a\in\mathcal{A}_r} d_a\}$, which calculates the optimal cost for a vehicle with configuration h running on route r without en-route charging. In addition, when $\alpha_h^0 = 0$ and $p_h = 0$ (i.e., indicating the utilization of diesel vehicles), (30) and (31) further reduce to $z_{h,r} \geq D\sum_{a\in\mathcal{A}_r} d_a$, which calculates the cost for a diesel vehicle running on route r.

This remark leads to the following observation: by incorporating (30) and (31) into the MP, we do not have to solve the dual subproblem $\mathrm{DSP}_{h,r}(\bar{\boldsymbol{x}}, \bar{\boldsymbol{y}})$ or $\text{PO-DSP}_{h,r}(\bar{\boldsymbol{x}}, \bar{\boldsymbol{y}}, \zeta_{h,r}, \boldsymbol{x}^c, \boldsymbol{y}^c)$ within the Benders decomposition framework for any vehicle configuration $h \in \mathcal{H}$ and route $r \in \mathcal{R}$ if $p_h = 0$ or $\mathcal{V}_r^1(\bar{\boldsymbol{y}}) = \varnothing$.

5.3 Subproblem reduction

The standard Benders decomposition requires solving $|\mathcal{H}| \times |\mathcal{R}|$ subproblems in each iteration for separating Benders cuts. For large-scale instances, the number of subproblems can be very large (in our experiments, this number can be greater than 1,000), creating significant computational burdens.

By incorporating inequalities (30) and (31), as indicated by Remark 1, one can avoid solving subproblems $\mathrm{DSP}_{h,r}(\bar{\boldsymbol{x}}, \bar{\boldsymbol{y}})$ or $\text{PO-DSP}_{h,r}(\bar{\boldsymbol{x}}, \bar{\boldsymbol{y}}, \zeta_{h,r}, \boldsymbol{x}^c, \boldsymbol{y}^c)$ for any $r \in \mathcal{R}$ or $h \in \mathcal{H}$ where either $\mathcal{V}_r^1(\bar{\boldsymbol{y}}) = \varnothing$ or $p_h = 0$. This section will discuss methods that further reduce the computational burden associated with solving subproblems and how to refine the cut separation process within the algorithm by using these methods.

5.3.1 Subproblem elimination

Given a solution $(\bar{\boldsymbol{x}}, \bar{\boldsymbol{y}}) \in \mathbf{X}$ to the MP, to reduce the number of subproblems $\mathrm{DSP}_{h,r}(\bar{\boldsymbol{x}}, \bar{\boldsymbol{y}})$ that need to be solved for a given route $r \in \mathcal{R}$, we group these subproblems across configurations $h \in \mathcal{H}$ such that the subproblems in a group share the same optimal solution. This is achieved by classifying the vertices included in route r into clusters, each characterized by unique charging speeds applicable to vehicles of specific configuration h.

Denoting the vertices along route r as $\mathcal{V}_r = \bigcup_{i\in\mathcal{N}_r}\{v(i)\}$, we then define, for a given $h \in \mathcal{H}$ and for each charging station type $k \in \mathcal{K}$, the set $\mathcal{V}_{h,r,k}(\bar{\boldsymbol{y}}) = \{v \in \mathcal{V}_r | \bar{y}_{k,v} = 1, g_k \leq p_h\}$ to represent vertices where the available charging speed g_k is no greater than charging rate p_h of configuration h. Additionally, we define $\mathcal{V}_{h,r,0}(\bar{\boldsymbol{y}}) = \{v \in \mathcal{V}_r | \bar{y}_{k,v} = 1, g_k > p_h, k \in \mathcal{K}\}$ to represent vertices where the charging speed of the station type exceeds the configuration's charging rate.

Given two solutions $(\bar{\boldsymbol{x}}^1, \bar{\boldsymbol{y}}^1), (\bar{\boldsymbol{x}}^2, \bar{\boldsymbol{y}}^2) \in \mathbf{X}$ to the MP, consider a particular route $r \in \mathcal{R}$ and a vehicle configuration $h \in \mathcal{H}$. Assume the following conditions are satisfied: (i) $\mathcal{V}_{h,r,k}(\bar{\boldsymbol{y}}^1) = \mathcal{V}_{h,r,k}(\bar{\boldsymbol{y}}^2), \forall k \in \mathcal{K}$, and (ii) $\mathcal{V}_{h,r,0}(\bar{\boldsymbol{y}}^1) = \mathcal{V}_{h,r,0}(\bar{\boldsymbol{y}}^2)$. Let $\zeta_{h,r}(\bar{\boldsymbol{x}}^1, \bar{\boldsymbol{y}}^1)$ and $\zeta_{h,r}(\bar{\boldsymbol{x}}^2, \bar{\boldsymbol{y}}^2)$ be the optimal objective function values for the dual subproblem $\mathrm{DSP}_{h,r}(\bar{\boldsymbol{x}}^1, \bar{\boldsymbol{y}}^1)$ and $\mathrm{DSP}_{h,r}(\bar{\boldsymbol{x}}^2, \bar{\boldsymbol{y}}^2)$, respective. We have the following lemma:

Lemma 1. For any $h \in \mathcal{H}$ and $r \in \mathcal{R}$, if conditions (i) and (ii) are met for two solutions $(\bar{\boldsymbol{x}}^1, \bar{\boldsymbol{y}}^1)$ and $(\bar{\boldsymbol{x}}^2, \bar{\boldsymbol{y}}^2)$, then $\zeta_{h,r}(\bar{\boldsymbol{x}}^1, \bar{\boldsymbol{y}}^1) = \zeta_{h,r}(\bar{\boldsymbol{x}}^2, \bar{\boldsymbol{y}}^2)$.

Additionally, let $\bar{\boldsymbol{\chi}}^1_{h,r}$ denote an optimal solution to $\text{PO-DSP}_{h,r}(\bar{\boldsymbol{x}}^1, \bar{\boldsymbol{y}}^1, \zeta^1_{h,r}, \boldsymbol{x}^c, \boldsymbol{y}^c)$ for any core point $(\boldsymbol{x}^c, \boldsymbol{y}^c)$. We further have the following proposition:

Proposition 3. $\bar{\boldsymbol{\chi}}^1_{h,r}$ is also an optimal solution to the problem $\text{PO-DSP}_{h,r}(\bar{\boldsymbol{x}}^2, \bar{\boldsymbol{y}}^2, \zeta^2_{h,r}, \boldsymbol{x}^c, \boldsymbol{y}^c)$.

This proposition leads to the following corollary:

Corollary 1. The Benders optimality cut

$$z_{h,r} \geq \sum_{i\in\mathcal{N}_r} w_i \bar{\eta}^1_i + \sum_{l\in\mathcal{L}_r} T_l \bar{\theta}^1_l + \sum_{a\in\mathcal{A}_r} d_a \bar{\vartheta}^1_a + \alpha^0_h \bar{\kappa}^1 + \sum_{i\in\mathcal{N}_r} q_h \bar{\psi}^1_i + \sum_{k\in\mathcal{K}} \sum_{i\in\mathcal{N}_r} M^1_{h,k,i} \bar{\varrho}^1_{i,k} y_{k,v(i)}$$

is valid, tight at $(\bar{\boldsymbol{x}}^2, \bar{\boldsymbol{y}}^2)$, and Pareto-optimal.

Corollary 1 implies that in any iteration $m \geq 1$ of the Benders decomposition algorithm, subproblems $\mathrm{DSP}_{h,r}(\bar{\boldsymbol{x}}^2, \bar{\boldsymbol{y}}^2)$ can be disregarded as long as we have $\bar{\boldsymbol{\chi}}^1_{h,r} \in \mathbf{P}^{m-1}(\Lambda_{h,r})$, where $\mathbf{P}^m(\Lambda_{h,r})$ represents the set of Benders cuts in iteration m, with $\mathbf{P}^0(\Lambda_{h,r}) = \varnothing$. Therefore, in each iteration of the Benders decomposition algorithm, before solving the subproblems, a subproblem elimination procedure is conducted. Details of the procedure are explained in EC.3.2 of the electronic companion.

5.3.2 Subproblem grouping

The number of subproblems that need to be solved in each iteration can be further reduced by partitioning the set $\mathcal{R} \times \mathcal{H}$ into groups such that the associated $\mathrm{DSP}_{h,r}$ in each group have an identical optimal solution, facilitating further subproblem reduction. We propose two grouping methods for this purpose: *Static Grouping*, which generates subsets of $\mathcal{R} \times \mathcal{H}$ prior to solving any subproblems, and *Dynamic Grouping*, which creates subsets of $\mathcal{R} \times \mathcal{H}$ using the information gathered from solving the subproblems.

Static Grouping. Given any MP solution $(\bar{\boldsymbol{x}}, \bar{\boldsymbol{y}}) \in \mathbf{X}$, for a specific route $r \in \mathcal{R}$, consider two configurations $h_1, h_2 \in \mathcal{H}$ such that: (i) $\alpha^0_{h_1} = \alpha^0_{h_2}$ (i.e., identical initial battery charges), (ii) $q_{h_1} = q_{h_2}$ (i.e., identical battery capacities), and (iii) $p_{h_1}, p_{h_2} \geq \max_{v\in\mathcal{V}_r} \sum_{k\in\mathcal{K}} \bar{y}_{k,v} g_k$ (i.e., charging speeds no slower than the maximum charging speed of the deployed charging stations on the route). Let $\zeta_{h_1,r}(\bar{\boldsymbol{x}}, \bar{\boldsymbol{y}})$ and $\zeta_{h_2,r}(\bar{\boldsymbol{x}}, \bar{\boldsymbol{y}})$ be the optimal objective function values for $\mathrm{DSP}_{h_1,r}(\bar{\boldsymbol{x}}, \bar{\boldsymbol{y}})$ and $\mathrm{DSP}_{h_2,r}(\bar{\boldsymbol{x}}, \bar{\boldsymbol{y}})$, respectively. Then, the following lemma holds:

Lemma 2. $\zeta_{h_1,r}(\bar{\boldsymbol{x}}, \bar{\boldsymbol{y}}) = \zeta_{h_2,r}(\bar{\boldsymbol{x}}, \bar{\boldsymbol{y}})$.

Furthermore, let $\bar{\boldsymbol{\chi}}_{h_1,r}$ represent an optimal solution to the Pareto-optimal dual problem $\text{PO-DSP}_{h_1,r}(\bar{\boldsymbol{x}}, \bar{\boldsymbol{y}}, \zeta_{h_1,r}, \boldsymbol{x}^c, \boldsymbol{y}^c)$ for any core point $(\boldsymbol{x}^c, \boldsymbol{y}^c)$. Suppose that we additionally have the condition: (iv) $p_{h_1} \geq p_{h_2}$ (i.e., charging speed of h_1 is no slower than that of h_2). Then, the following proposition is true:

Proposition 4. $\bar{\boldsymbol{\chi}}_{h_1,r}$ is a feasible solution to $\text{PO-DSP}_{h_2,r}(\bar{\boldsymbol{x}}, \bar{\boldsymbol{y}}, \zeta_{h_2,r}, \boldsymbol{x}^c, \boldsymbol{y}^c)$.

Proposition 4 also indicates that we can obtain a valid Benders optimality cut for $z_{h_2,r}$ based on the solution $\bar{\boldsymbol{\chi}}_{h_1,r}$. The following corollary shows that this cut is tight.

Corollary 2. The Benders optimality cut

$$z_{h_2,r} \geq \sum_{i\in\mathcal{N}_r} w_i \bar{\eta}_i + \sum_{l\in\mathcal{L}_r} T_l \bar{\theta}_l + \sum_{a\in\mathcal{A}_r} d_a \bar{\vartheta}_a + \alpha^0_h \bar{\kappa} + \sum_{i\in\mathcal{N}_r} q_{h_1} \bar{\psi}_i + \sum_{k\in\mathcal{K}} \sum_{i\in\mathcal{N}_r} M_{h_1,k,i} \bar{\varrho}_{i,k} y_{k,v(i)}$$

is valid and tight at $(\bar{\boldsymbol{x}}, \bar{\boldsymbol{y}})$.

Remark 2. In EV operations optimization, two assumptions are common: (a) all electrical vehicles are charged to the same level of electricity at the depot; and (b) vehicles start their routes with their batteries charged to a specific fraction of their total capacities. Condition (i) holds when (a) is true or when conditions (ii) and (b) are true.

Using these results, in each iteration of the Benders decomposition algorithm, given a solution $(\bar{\boldsymbol{x}}, \bar{\boldsymbol{y}}) \in \mathbf{X}$ to the MP and a route $r \in \mathcal{R}$, we partition the configuration set $\mathcal{H}$ into a group $\mathcal{J}_r$ of subsets $\mathcal{H}_{r,j}$ such that $\bigcup_{j\in\mathcal{J}_r} \mathcal{H}_{r,j} = \mathcal{H}$. Note that given any group $j \in \mathcal{J}_r$, $\mathcal{H}_{r,j}$ can be a singleton containing only one configuration $h \in \mathcal{H}$. For any $j \in \mathcal{J}_r : |\mathcal{H}_{r,j}| \geq 2$, the following conditions must be satisfied: (i) $\alpha^0_{h_1} = \alpha^0_{h_2}$, $\forall h_1, h_2 \in \mathcal{H}_{r,j}$, (ii) $q_{h_1} = q_{h_2}$, $\forall h_1, h_2 \in \mathcal{H}_{r,j}$, and (iii) $p_h \geq \max_{v\in\mathcal{V}_r} \sum_{k\in\mathcal{K}} \bar{y}_{k,v} g_k$, $\forall h \in \mathcal{H}_{r,j}$.

Let $h_0 = \arg\max_{h\in\mathcal{H}_{r,j}}\{p_h\}$ where $j \in \mathcal{J}_r$, $r \in \mathcal{R}$, Lemma 2 indicates that only one primal or dual subproblem (i.e., $\text{PSP}_{h_0,r}(\bar{\boldsymbol{x}}, \bar{\boldsymbol{y}})$ or $\text{DSP}_{h_0,r}(\bar{\boldsymbol{x}}, \bar{\boldsymbol{y}})$) has to be solved to check whether new Benders optimality cuts should be separated for $z_{h,r}$, $\forall h \in \mathcal{H}_{r,j}$. Furthermore, from Corollary 2, in theory, the Benders cut generated by solving the Pareto-optimal dual subproblem $\text{PO-DSP}_{h_0,r}(\bar{\boldsymbol{x}}, \bar{\boldsymbol{y}}, \zeta_{h_0,r}, \boldsymbol{x}^c, \boldsymbol{y}^c)$ is sufficient for bounding any decision variables $z_{h,r}$ with $h \in \mathcal{H}_{r,j}$.

Dynamic Grouping. Given any MP solution $(\bar{\boldsymbol{x}}, \bar{\boldsymbol{y}}) \in \mathbf{X}$, let $\bar{\boldsymbol{\alpha}}_{h,r}$ and $\bar{\boldsymbol{\beta}}_{h,r}$ denote the values of $\alpha_{h,i}$ and $\beta_{h,i}$ variables in an optimal solution to the primal subproblem $\text{PSP}_{h,r}(\bar{\boldsymbol{x}}, \bar{\boldsymbol{y}})$ such that

$$\bar{\alpha}_{h,i} + \bar{\beta}_{h,i} < q_h \qquad \forall i \in \mathcal{N}_r, \tag{32}$$

where $h \in \mathcal{H}$, $r \in \mathcal{R}$. Given this property, we have the following lemma.

Lemma 3. Supposing that (32) holds for an optimal solution of $\text{PSP}_{h,r}(\bar{\boldsymbol{x}}, \bar{\boldsymbol{y}})$, where $h \in \mathcal{H}$, $r \in \mathcal{R}$, there exists a feasible solution, denoted by $\bar{\boldsymbol{\chi}}_{h,r}$, to the Pareto-optimal dual subproblem $\text{PO-DSP}_{h,r}(\bar{\boldsymbol{x}}, \bar{\boldsymbol{y}}, \zeta_{h_1,r}, \boldsymbol{x}^c, \boldsymbol{y}^c)$ such that $\bar{\boldsymbol{\psi}}_{h,r} = \mathbf{0}$, where $(\boldsymbol{x}^c, \boldsymbol{y}^c)$ is a core point.

Given $(\bar{\boldsymbol{x}}, \bar{\boldsymbol{y}}) \in \mathbf{X}$, suppose that we have $h_1, h_2 \in \mathcal{H}$ and $r \in \mathcal{R}$ such that: (i) (32) holds for an optimal solution of $\text{PSP}_{h_1,r}(\bar{\boldsymbol{x}}, \bar{\boldsymbol{y}})$, (ii) $\alpha^0_{h_1} = \alpha^0_{h_2}$ (i.e., identical initial battery charges), (iii) $q_{h_1} \leq q_{h_2}$ (i.e., battery capacity of h_1 is no smaller than that of h_2), and (iv) $p_{h_1}, p_{h_2} \geq \max_{v\in\mathcal{V}_r} \sum_{k\in\mathcal{K}} \bar{y}_{k,v} g_k$ (i.e., charging speeds no slower than the maximum charging speed of the deployed charging stations on the route). Let $\zeta_{h_1,r}(\bar{\boldsymbol{x}}, \bar{\boldsymbol{y}})$ and $\zeta_{h_2,r}(\bar{\boldsymbol{x}}, \bar{\boldsymbol{y}})$ be the optimal objective function values to $\text{PSP}_{h_1,r}(\bar{\boldsymbol{x}}, \bar{\boldsymbol{y}})$ and $\text{PSP}_{h_2,r}(\bar{\boldsymbol{x}}, \bar{\boldsymbol{y}})$, respectively. Then we have the following lemma:

Lemma 4. $\zeta_{h_1,r}(\bar{\boldsymbol{x}}, \bar{\boldsymbol{y}}) = \zeta_{h_2,r}(\bar{\boldsymbol{x}}, \bar{\boldsymbol{y}})$.

Following Lemma 3, let $\bar{\boldsymbol{\chi}}_{h_1,r}$ with $\bar{\boldsymbol{\psi}}_{h_1,r} = \mathbf{0}$ denote a feasible solution to the Pareto-optimal dual subproblem $\text{PO-DSP}_{h_1,r}(\bar{\boldsymbol{x}}, \bar{\boldsymbol{y}}, \zeta_{h_1,r}, \boldsymbol{x}^c, \boldsymbol{y}^c)$, where $(\boldsymbol{x}^c, \boldsymbol{y}^c)$ is a core point. Suppose that we have the additional condition (v) $p_{h_1} \geq p_{h_2}$ (i.e., charging speed of h_1 is no slower than that of h_2). Then the following proposition holds.

Proposition 5. $\bar{\boldsymbol{\chi}}_{h_1,r}$ is also a feasible solution to $\text{PO-DSP}_{h_2,r}(\bar{\boldsymbol{x}}, \bar{\boldsymbol{y}}, \zeta_{h_2,r}, \boldsymbol{x}^c, \boldsymbol{y}^c)$.

Again, the following corollary shows that the associated Benders cut for $z_{h_2,r}$ is valid and tight.

Corollary 3. The Benders optimality cut

$$z_{h_2,r} \geq \sum_{i\in\mathcal{N}_r} w_i \bar{\eta}_i + \sum_{l\in\mathcal{L}_r} T_l \bar{\theta}_l + \sum_{a\in\mathcal{A}_r} d_a \bar{\vartheta}_a + \alpha^0_h \bar{\kappa} + \sum_{i\in\mathcal{N}_r} q_{h_1} \bar{\psi}_i + \sum_{k\in\mathcal{K}} \sum_{i\in\mathcal{N}_r} M_{h_1,k,i} \bar{\varrho}_{i,k} y_{k,v(i)}$$

is valid and tight at $(\bar{\boldsymbol{x}}, \bar{\boldsymbol{y}})$.

Furthermore, if we have (vi) $p_{h_1} = p_{h_2}$ (i.e., identical charging speeds), then the following proposition holds.

Proposition 6. The Benders optimality cut

$$z_{h_2,r} \geq \sum_{i\in\mathcal{N}_r} w_i \bar{\eta}_i + \sum_{l\in\mathcal{L}_r} T_l \bar{\theta}_l + \sum_{a\in\mathcal{A}_r} d_a \bar{\vartheta}_a + \alpha^0_h \bar{\kappa} + \sum_{i\in\mathcal{N}_r} q_{h_1} \bar{\psi}_i + \sum_{k\in\mathcal{K}} \sum_{i\in\mathcal{N}_r} M_{h_1,k,i} \bar{\varrho}_{i,k} y_{k,v(i)}$$

is valid, tight at $(\bar{\boldsymbol{x}}, \bar{\boldsymbol{y}})$, and Pareto-optimal.

To incorporate dynamic subproblem grouping into the Benders decomposition algorithm, after solving each subproblem, we look for configurations that meet the conditions (i)−(iv). Specifically, in each iteration m of the Benders decomposition algorithm, we obtain a solution $(\bar{\boldsymbol{x}}, \bar{\boldsymbol{y}}) \in \mathbf{X}$ to the MP. Let $\bar{\boldsymbol{\alpha}}_{h,r}$ and $\bar{\boldsymbol{\beta}}_{h,r}$ represent the vectors of $\alpha_{h,i}$ and $\beta_{h,i}$ values in an optimal solution to the primal subproblem $\text{PSP}_{h,r}(\bar{\boldsymbol{x}}, \bar{\boldsymbol{y}})$, where $h \in \mathcal{H}$ and $r \in \mathcal{R}$. If $p_h \geq \max_{v \in \mathcal{V}_r} \sum_{k \in \mathcal{K}} \bar{y}_{k,v} g_k$ and inequalities (32) hold, we then define a set $\mathcal{H}'_{h,r}$ such that $\mathcal{H}'_{h,r} = \{h' \in \mathcal{H} | \alpha^0_{h'} = \alpha^0_h, q_{h'} \geq q_h, p_{h'} \geq \max_{v \in \mathcal{V}_r} \sum_{k \in \mathcal{K}} \bar{y}_{k,v} g_k\}$. Then, Lemma 4 indicates that only one primal subproblem (i.e., $\text{PSP}_{h,r}(\bar{\boldsymbol{x}}, \bar{\boldsymbol{y}})$) has to be solved to check whether new Benders optimality cuts should be separated for $z_{h,r}$, $\forall h \in \mathcal{H}'_{r,j}$.

In addition, let $\bar{\boldsymbol{\psi}}_{h,r}$ denote the vector for the values of ψ_i variables in the optimal solution to $\text{PO-DSP}_{h,r}(\bar{\boldsymbol{x}}, \bar{\boldsymbol{y}}, \zeta_{h,r}, \boldsymbol{x}^c, \boldsymbol{y}^c)$. If $\bar{\boldsymbol{\psi}}_{h,r} = \mathbf{0}$ and $p_h \geq p_{h'}$, Corollary 3 suggests that the Benders optimality cut derived from the solution to $\text{PO-DSP}_{h,r}(\bar{\boldsymbol{x}}, \bar{\boldsymbol{y}}, \zeta_{h,r}, \boldsymbol{x}^c, \boldsymbol{y}^c)$ is valid and tight for all $z_{h',r}$, with $h' \in \mathcal{H}'_{h,r}$.

5.3.3 Benders cut separation with subproblem reduction

In each iteration of the Benders decomposition algorithm, each separation procedure begins by running the subproblem elimination routine to reduce the number of subproblems (refer to EC.3.2 for more details). Let $\mathbb{I}_{h,r}$ be the indicators presenting validity of subproblems $\text{PSP}_{h,r}(\bar{\boldsymbol{x}}, \bar{\boldsymbol{y}})$ returned by the elimination routine, where $(\bar{\boldsymbol{x}}, \bar{\boldsymbol{y}}) \in \mathbf{X}$ is the solution to the MP in the iteration.

Then, for each route $r \in \mathcal{R}$, we apply the static grouping method to partition the subproblems associated with configurations $h \in \mathcal{H} : \mathbb{I}_{h,r} = 1$ into a set $\mathcal{J}_r$ of groups. For each group $j \in \mathcal{J}_r$ and route $r \in \mathcal{R}$, we solve the primal subproblem $\text{PSP}_{h^0_j,r}(\bar{\boldsymbol{x}}, \bar{\boldsymbol{y}})$, where $h^0_j = \arg\max_{h \in \mathcal{H}_{r,j}} \{p_h\}$. Subsequently, dynamic grouping is applied based on the solution of $\text{PSP}_{h^0_j,r}(\bar{\boldsymbol{x}}, \bar{\boldsymbol{y}})$ to reduce the number of groups in $\mathcal{J}_r$ with subproblems needing to be solved. Finally, we separate Benders cuts for the resulting groups by jointly applying Corollaries 2 and 3.

Observe that Corollaries 2 and 3 demonstrate that the Benders cuts generated by static and dynamic grouping are valid and tight. This ensures the convergence of the Benders decomposition algorithm when only cuts such separated are incorporated in the algorithm. However, unless the conditions of Proposition 6 are satisfied, the Benders cuts generated by static and dynamic grouping are not necessarily Pareto-optimal. To generate "stronger" Benders cuts, we first identify, from subproblems in a group, those where Corollaries 2 or 3 are more likely to lead to strong Benders cuts. For these subproblems, the corresponding Benders cuts (if any) are separated by directly applying the two corollaries, without solving their associated Pareto-optimal subproblems. Then, for the remaining subproblems, whenever needed, their corresponding Pareto-optimal subproblems are solved to generate Pareto-optimal Benders cuts. Details of the separation procedure are explained in EC.3.3 of the electronic companion.

5.4 Benders-based branch-and-cut

As outlined in Algorithm EC.2 of EC.3.1, in each iteration m, the standard Benders decomposition routine solves the MP and then separates Benders cuts by solving the subproblems. The separated cuts will be incorporated into an updated collection of Benders optimality cuts, denoted as $\mathbf{P}^m(\Lambda_{h,r})$. To solve the MP in each iteration, a branch-and-bound tree has to be constructed from scratch, which can be time-consuming.

To mitigate the computational burden of repeatedly solving the MP, we introduce a branch-and-cut strategy tailored to the Benders reformulation. This approach necessitates the construction of a single branch-and-bound tree for the MP, where Benders optimality cuts are separated at various nodes within the tree. This method has been successfully implemented in prior studies (e.g., Botton et al. 2013), to enhance the efficiency of the Benders decomposition technique. In our application, Benders cuts are separated at nodes that yield an integer solution to the MP.

6 Computational experiments

We conducted extensive computational experiments to assess the practicality and proficiency of the solution approach. These experiments were designed based on a practical electrification project faced by our industrial partner. Section 6.1 introduces the specifics of these instances. The experiments consisted of two parts. The first part examined the performance of the solution algorithm, while the second part investigated the benefits of electrification. Their results are reported in Sections 6.2 and 6.3, respectively.

We coded the algorithms in C++, and conducted the experiments on the Cedar cluster of Compute Canada, which was operated in a Linux environment with 128G RAM on a single thread. We used CPLEX 20.1.0 to solve the MILP and LP models. For any instance, we allocated a time limit of 24 hours (1,440 minutes) for each solution method. The codes, data sets, and detailed results are provided in the link.[7]

6.1 Problem instances

The instances were inspired by a HDV electrification project from our industrial partner. The project aimed at electrifying diesel container trucks at a major Canadian seaport. We collected data from the project, which can be classified into two categories: electrification technical parameters and fleet GPS records. Using the technical data, we derived 22 truck electrification configurations, each characterized by a unique combination of a battery capacity, a default charging speed, and an electrification cost. Additionally, there were three types of ground charging stations associated with different default charging speeds and set-up costs. To formulate the problem, the terminal area of the seaport was represented as a graph $\mathcal{G} = (\mathcal{V}, \mathcal{E})$ with $|\mathcal{V}| = 56$ and $|\mathcal{E}| = 144$. The terminal operated a homogeneous fleet of 50 diesel trucks. These trucks run around the clock. Using the collected GPS records of these trucks, we generated 309 routes on graph $\mathcal{G}$, each representing a truck's four-hour shift operations. Each route contains 207 nodes on average.

Notably, one of the 22 configurations represents the non-electrification option. Any truck with this configuration is run in the original diesel mode. Furthermore, we set the budget (in US dollars) for electrification as $B = 10,000 \times F$, where F represents the fleet size in an instance.

We generated four instance configurations, differing in the requirements of fleet composition and buffer time for vehicle charging. In particular, for fleet composition, let Γ be the indicator for the homogeneity requirements, such that $\Gamma = 1$ indicates that all vehicles in an instance should be retrofitted with the same configuration and $\Gamma = 0$ indicates that a heterogeneous fleet is allowed. Meanwhile, for the buffer time of vehicle charging, we introduced δ as the buffer time ratio, such that the travel times of legs are set as $T_l = (1 + \delta) \sum_{i \in \mathcal{N}_l} w_i$, for all $l \in \mathcal{L}$ in an instance. We tested the δ taking values in $\{0\%, 5\%\}$. Furthermore, when solving instances with $\Gamma = 1$ we incorporated two additional constraints into the feasible region of electrification decisions ($\mathbf{X}$) for imposing the homogeneity of the fleet: (i) $\sum_{f=1}^{F-1} \sum_{h \in \mathcal{H}} x_{f,h} = 0$ and (ii) $\sum_{h \in \mathcal{H}} x_{F,h} = 1$.

All test instances were generated using the same graph $\mathcal{G}$, and we have $|\mathcal{H}| = 22$ and $|\mathcal{K}| = 3$ across all instances. Each instance has a planning horizon of 10 years. On top of Γ and δ, the instances further differ in the size of the route sample set $\mathcal{R}$ and the fleet size F. We varied $|\mathcal{R}|$ within $\{10, 20, 30, 40, 50\}$ and F within $\{10, 20, 40, 50\}$. In total, 20 combinations of $|\mathcal{R}|$ and F were examined. For the configurations with $\Gamma = 1$ and $\delta \in \{0\%, 5\%\}$, we tested all combinations with $|\mathcal{R}| \in \{10, 20, 30, 40, 50\}$ and $F \in \{10, 20, 40, 50\}$. Additionally, due to escalated computational complexity, for the configurations with $\Gamma = 0$ and $\delta \in \{0\%, 5\%\}$, we tested combinations with $|\mathcal{R}| \in \{10, 20\}$ and $F \in \{10, 20, 30, 40, 50\}$.

In total, 60 combinations of parameters $(\Gamma, F, |\mathcal{R}|, \delta)$ were tested in the experiments. Of these, 40 combinations include fleet homogeneity requirements (i.e., $\Gamma = 1$), while the remaining 20 do not

[7] https://github.com/Optimization2025/EPPOC.

(i.e., $\Gamma = 0$). For each combination, we generated five instances by randomly creating route samples, resulting in a total of 300 instances. These instances were used in the first part of the experiments for assessing the computational performance of the Benders decomposition algorithm.

6.2 Computational performance

We implemented three variants of the Benders decomposition algorithm to assess the performance of our computational enhancements:

1. BD1, applying the basic Benders decomposition algorithm outlined in EC.3.1 within a branch-and-cut framework as described in Section 5.4;
2. BD2, which extends BD1 by incorporating Pareto-optimality cuts from Section 5.1;
3. BD3, building on BD2 by including lower-bound lifting inequalities and subproblem reduction strategies from Sections 5.2 and 5.3.

On top of these, we also ran CPLEX on the MILP model M1 to solve these instances. In Section 6.2.1, we present the computational results of CPLEX and BD3. Section 6.2.2 compares the results of the three Benders decomposition algorithm variants. The result tables in this section share the same structure. For each group of five instances that share the same setting of Γ, δ, F, and $|\mathcal{R}|$, we report the number of instances solved to optimality (in column *Opt*), the average optimality gap in percentage (in column *Gap*), and the average CPU time in minutes (in column *Time*). Row *Total* reports the total number of instances solved to optimality, the average optimality gap, and average solution time for all instances with the same Γ and δ.

6.2.1 Comparisons with solver on the original MILP

Table 1 reports the results delivered by CPLEX on model M1 and BD3 on 200 instances with fleet homogeneity requirements (i.e., $\Gamma = 1$). These instances are classified into 40 groups.

As shown in Table 1, for instances with fleet homogeneity requirements (i.e., $\Gamma = 1$), CPLEX was able to generate optimal solutions for all instances with zero buffer charging times (i.e., $\delta = 0\%$) within short computational times. However, its performance on instances with non-zero buffer charging times (i.e., $\delta = 5\%$) was significantly worse. In particular, less than half of the instances were solved to optimality within the time limit (1,440 minutes) and the average optimality gap exceeded 40% for a group. In comparison, BD3 demonstrates significant superiority for all instance groups. It also managed to solve all instances with $\delta = 0\%$ to optimality and provided optimality certificates to 86 of the 100 instances with $\delta = 5\%$. Additionally, the average optimality gaps for all instances reported by BD3 were within 1%. As for the efficiency, for instance groups where both CPLEX and BD3 obtained optimal solutions for all instances, BD3 reported solution times that were one-to-two orders of magnitude smaller than those reported by CPLEX.

Table 2 summarizes the results produced by CPLEX and BD3 on 100 instances without fleet homogeneity requirements (i.e., $\Gamma = 0$). These instances are classified into 20 groups. The data presented in Table 2 indicates that the EPPOC becomes more computationally challenging when the fleet homogeneity constraints are relaxed (i.e., $\Gamma = 0$). Similar to the results on instances with $\Gamma = 1$, both CPLEX and BD3 exhibited better performance on instances with zero buffer charging times (i.e., $\delta = 0\%$) compared to those with non-zero buffer charging times (i.e., $\delta = 5\%$). Furthermore, BD3 dominated CPLEX with respect to both solution quality and computational efficiency. Specifically, BD3 delivered optimal solutions to 48 and 14 instances with $\delta = 0\%$ and $\delta = 5\%$, respectively, while CPLEX reported only 19 and 3 instances with $\delta = 0\%$ and $\delta = 5\%$, respectively. The average optimality gaps for BD3 are notably lower, standing at 0.0% for instances with $\delta = 0\%$ and 3.4% for those with $\delta = 5\%$. On the other hand, the average optimality gaps for CPLEX are 5.2% for $\delta = 0\%$ instances and 17.5% for $\delta = 5\%$ instances. When it comes to computational speed, BD3 consistently delivered quicker average computation times across most instance groups. Notably, for smaller instances with $F = 10$, the speed advantage of BD3 over CPLEX is even more pronounced, with BD3 being significantly faster by several orders of magnitude.

Table 1: Computational results of CPLEX and BD3 on instances with $\Gamma = 1$.

$(F, \|\mathcal{R}\|, \delta)$	CPLEX			BD3			$(F, \|\mathcal{R}\|, \delta)$	CPLEX			BD3		
	Opt	Gap	Time	Opt	Gap	Time		Opt	Gap	Time	Opt	Gap	Time
(10,10,0)	5	0.0	0.4	5	0.0	0.0	(10,10,5)	5	0.0	48.2	5	0.0	0.7
(10,20,0)	5	0.0	0.9	5	0.0	0.0	(10,20,5)	5	0.0	302.7	5	0.0	2.6
(10,40,0)	5	0.0	4.8	5	0.0	0.1	(10,40,5)	1	8.7	1369.1	5	0.0	13.2
(10,50,0)	5	0.0	6.8	5	0.0	0.1	(10,50,5)	0	41.4	1440.0	5	0.0	16.1
(20,10,0)	5	0.0	0.8	5	0.0	0.1	(20,10,5)	5	0.0	114.1	5	0.0	15.3
(20,20,0)	5	0.0	3.1	5	0.0	0.2	(20,20,5)	3	0.6	1009.0	5	0.0	195.6
(20,40,0)	5	0.0	6.1	5	0.0	0.2	(20,40,5)	0	7.3	1440.0	4	0.2	782.4
(20,50,0)	5	0.0	9.0	5	0.0	0.2	(20,50,5)	0	36.9	1440.0	2	1.0	959.7
(30,10,0)	5	0.0	0.6	5	0.0	0.1	(30,10,5)	5	0.0	176.4	5	0.0	17.5
(30,20,0)	5	0.0	2.6	5	0.0	0.1	(30,20,5)	1	1.0	1204.5	3	0.2	724.4
(30,40,0)	5	0.0	8.8	5	0.0	0.4	(30,40,5)	0	19.9	1440.0	3	0.6	1051.7
(30,50,0)	5	0.0	9.1	5	0.0	0.2	(30,50,5)	0	22.9	1440.0	4	0.2	812.0
(40,10,0)	5	0.0	0.9	5	0.0	0.1	(40,10,5)	5	0.0	173.1	5	0.0	38.2
(40,20,0)	5	0.0	2.2	5	0.0	0.1	(40,20,5)	4	0.2	604.9	4	0.0	330.1
(40,40,0)	5	0.0	6.6	5	0.0	0.2	(40,40,5)	1	5.1	1424.1	4	0.4	763.4
(40,50,0)	5	0.0	8.5	5	0.0	0.3	(40,50,5)	0	27.3	1440.0	4	0.3	733.7
(50,10,0)	5	0.0	0.9	5	0.0	0.1	(50,10,5)	5	0.0	54.0	5	0.0	27.2
(50,20,0)	5	0.0	1.7	5	0.0	0.1	(50,20,5)	5	0.0	212.9	5	0.0	23.1
(50,40,0)	5	0.0	4.8	5	0.0	0.2	(50,40,5)	1	8.7	1401.9	4	0.1	583.2
(50,50,0)	5	0.0	9.6	5	0.0	0.3	(50,50,5)	0	16.8	1440.0	4	0.2	552.1
Total	100	0.0	4.4	100	0.0	0.2	Total	46	9.8	908.7	86	0.2	382.2

Table 2: Computational results of CPLEX and BD3 on instances with $\Gamma = 0$.

$(F, \|\mathcal{R}\|, \delta)$	CPLEX			BD3			$(F, \|\mathcal{R}\|, \delta)$	CPLEX			BD3		
	Opt	Gap	Time	Opt	Gap	Time		Opt	Gap	Time	Opt	Gap	Time
(10,10,0)	5	0.0	119.2	5	0.0	2.6	(10,10,5)	1	7.8	1286.6	5	0.0	16.6
(10,20,0)	1	2.9	1160.1	5	0.0	17.4	(10,20,5)	0	24.4	1440.0	5	0.0	140.9
(20,10,0)	4	1.3	610.9	5	0.0	36.9	(20,10,5)	1	14.2	1371.5	3	0.7	780.2
(20,20,0)	0	11.9	1440.0	5	0.0	552.0	(20,20,5)	0	29.7	1440.0	0	6.9	1440.0
(30,10,0)	5	0.0	728.0	5	0.0	160.1	(30,10,5)	1	15.2	1430.1	1	3.0	1186.3
(30,20,0)	1	9.9	1413.1	5	0.0	446.1	(30,20,5)	0	24.3	1440.0	0	5.9	1440.0
(40,10,0)	1	2.8	1353.6	5	0.0	104.5	(40,10,5)	0	17.8	1440.0	0	4.0	1440.0
(40,20,0)	0	11.6	1440.0	5	0.0	510.2	(40,20,5)	0	18.1	1440.0	0	4.9	1440.0
(50,10,0)	1	3.8	1181.8	5	0.0	599.8	(50,10,5)	0	13.8	1440.0	0	3.7	1440.0
(50,20,0)	1	7.6	1437.8	3	0.3	965.0	(50,20,5)	0	9.5	1440.0	0	4.6	1440.0
Total	19	5.2	1088.5	48	0.0	339.5	Total	3	17.5	1416.8	14	3.4	1076.4

6.2.2 Impacts of the computational enhancements

We further investigated the impacts of the computational enhancements proposed in Section 5 by comparing the performance of three variants of the Benders decomposition algorithm. Table 3 reports the computational results of these algorithms on instances with fleet homogeneity requirements (i.e., $\Gamma = 1$).

As shown in Table 3, all algorithms produced optimal solutions to all instances with zero buffer charging times. The speed-up between BD2 and BD1 and between BD3 and BD2 demonstrates the values of Pareto-optimal cuts and subproblem reduction, respectively. The impacts of the enhancements are more profound on instances with non-zero buffer charging times. Specifically, BD1 managed to find optimal solutions to 45 out of the 100 instances with $\delta = 5\%$, while BD2 and BD3 were able to deliver optimal solutions to 57 and 86 instances, respectively. Additionally, the average optimality gap is reduced from 1.5% to 0.8% and further to 0.2% by incorporating Pareto-optimal cuts and subproblem reduction into the algorithm, respectively. As for the computational efficiency, BD2 required less than half the computational time when compared with BD1 on instance groups where both methods delivered optimal solutions to all instances, which demonstrates the value of Pareto-optimal cuts. Additionally, on average, the subproblem reduction techniques provided a 6.9 times speed-up for nine groups of instances where both BD2 and BD3 found optimal solutions to all instances.

Table 3: Computational results of BD1, BD2, and BD3 on instances with $\Gamma = 1$.

$(F, \|\mathcal{R}\|, \delta)$	BD1			BD2			BD3			$(F, \|\mathcal{R}\|, \delta)$	BD1			BD2			BD3		
	Opt	Gap	Time	Opt	Gap	Time	Opt	Gap	Time		Opt	Gap	Time	Opt	Gap	Time	Opt	Gap	Time
(10,10,0)	5	0.0	0.1	5	0.0	0.1	5	0.0	0.0	(10,10,5)	5	0.0	11.1	5	0.0	5.1	5	0.0	0.7
(10,20,0)	5	0.0	0.0	5	0.0	0.1	5	0.0	0.0	(10,20,5)	5	0.0	72.7	5	0.0	21.3	5	0.0	2.6
(10,40,0)	5	0.0	0.2	5	0.0	0.3	5	0.0	0.1	(10,40,5)	4	0.3	709.8	5	0.0	94.1	5	0.0	13.2
(10,50,0)	5	0.0	0.3	5	0.0	0.3	5	0.0	0.1	(10,50,5)	5	0.0	731.3	5	0.0	120.0	5	0.0	16.1
(20,10,0)	5	0.0	0.3	5	0.0	0.3	5	0.0	0.1	(20,10,5)	3	0.8	664.0	5	0.0	315.4	5	0.0	15.3
(20,20,0)	5	0.0	0.6	5	0.0	0.5	5	0.0	0.2	(20,20,5)	1	2.5	1375.0	3	0.8	974.6	5	0.0	195.6
(20,40,0)	5	0.0	0.7	5	0.0	0.6	5	0.0	0.2	(20,40,5)	0	4.0	1440.0	0	2.4	1440.0	4	0.2	782.4
(20,50,0)	5	0.0	0.9	5	0.0	0.7	5	0.0	0.2	(20,50,5)	0	4.7	1440.0	0	3.2	1440.0	2	1.0	959.7
(30,10,0)	5	0.0	0.2	5	0.0	0.2	5	0.0	0.1	(30,10,5)	4	0.2	572.4	5	0.0	142.1	5	0.0	17.5
(30,20,0)	5	0.0	0.5	5	0.0	0.4	5	0.0	0.1	(30,20,5)	1	2.5	1163.7	1	1.6	1157.9	3	0.2	724.4
(30,40,0)	5	0.0	1.9	5	0.0	0.9	5	0.0	0.4	(30,40,5)	0	3.6	1440.0	0	2.1	1440.0	3	0.6	1051.7
(30,50,0)	5	0.0	1.1	5	0.0	0.8	5	0.0	0.2	(30,50,5)	0	2.8	1440.0	1	1.5	1362.6	4	0.2	812.0
(40,10,0)	5	0.0	0.5	5	0.0	0.2	5	0.0	0.1	(40,10,5)	4	0.3	1063.4	5	0.0	225.8	5	0.0	38.2
(40,20,0)	5	0.0	0.8	5	0.0	0.4	5	0.0	0.1	(40,20,5)	3	0.8	865.3	4	0.4	655.4	4	0.0	330.1
(40,40,0)	5	0.0	1.1	5	0.0	0.7	5	0.0	0.2	(40,40,5)	0	2.3	1440.0	0	1.4	1440.0	4	0.4	763.4
(40,50,0)	5	0.0	1.6	5	0.0	1.0	5	0.0	0.3	(40,50,5)	0	2.0	1440.0	1	1.2	1418.3	4	0.3	733.7
(50,10,0)	5	0.0	0.4	5	0.0	0.3	5	0.0	0.1	(50,10,5)	4	0.1	474.5	5	0.0	75.9	5	0.0	27.2
(50,20,0)	5	0.0	0.6	5	0.0	0.4	5	0.0	0.1	(50,20,5)	5	0.0	450.9	5	0.0	103.0	5	0.0	23.1
(50,40,0)	5	0.0	1.7	5	0.0	0.8	5	0.0	0.2	(50,40,5)	0	1.6	1440.0	0	0.8	1440.0	4	0.1	584.2
(50,50,0)	5	0.0	3.0	5	0.0	1.1	5	0.0	0.3	(50,50,5)	1	1.3	1321.4	2	0.8	1182.9	4	0.2	552.1
Total	100	0.0	0.8	100	0.0	0.5	100	0.0	0.2	Total	45	1.5	977.8	57	0.8	752.7	86	0.2	382.2

We further compare the performance of the three Benders decomposition algorithms on instances where the fleet homogeneity requirements are dropped (i.e., $\Gamma = 0$). Table 4 reports the corresponding results.

Table 4: Computational results of BD1, BD2, and BD3 on instances with $\Gamma = 0$.

$(F, \|\mathcal{R}\|, \delta)$	BD1			BD2			BD3			$(F, \|\mathcal{R}\|, \delta)$	BD1			BD2			BD3		
	Opt	Gap	Time	Opt	Gap	Time	Opt	Gap	Time		Opt	Gap	Time	Opt	Gap	Time	Opt	Gap	Time
(10,10,0)	5	0.0	28.8	5	0.0	3.7	5	0.0	2.6	(10,10,5)	5	0.0	391.4	5	0.0	302.7	5	0.0	16.6
(10,20,0)	5	0.0	104.0	5	0.0	16.3	5	0.0	17.4	(10,20,5)	0	6.4	1440.0	1	5.7	1421.9	5	0.0	140.9
(20,10,0)	4	1.1	585.0	5	0.0	44.2	5	0.0	36.9	(20,10,5)	1	9.2	1352.2	1	8.2	1426.5	3	0.7	780.2
(20,20,0)	0	8.8	1440.0	4	0.6	498.4	5	0.0	552.0	(20,20,5)	0	22.3	1440.0	0	17.9	1440.0	0	6.9	1440.0
(30,10,0)	1	6.8	1282.7	4	0.1	821.5	5	0.0	160.1	(30,10,5)	0	14.1	1440.0	0	11.7	1440.0	1	3.0	1186.3
(30,20,0)	0	10.3	1440.0	2	3.0	1242.0	5	0.0	446.1	(30,20,5)	0	21.0	1440.0	0	18.7	1440.0	0	5.9	1440.0
(40,10,0)	0	11.0	1440.0	0	3.5	1440.0	5	0.0	104.5	(40,10,5)	0	18.2	1440.0	0	14.7	1440.0	0	4.0	1440.0
(40,20,0)	0	14.2	1440.0	0	7.0	1440.0	5	0.0	510.2	(40,20,5)	0	20.0	1440.0	0	17.0	1440.0	0	4.9	1440.0
(50,10,0)	0	12.3	1440.0	0	6.3	1440.0	5	0.0	599.8	(50,10,5)	0	15.1	1440.0	0	13.6	1440.0	0	3.7	1440.0
(50,20,0)	0	13.3	1440.0	0	8.8	1440.0	3	0.3	965.0	(50,20,5)	0	19.0	1440.0	0	15.1	1440.0	0	4.6	1440.0
Total	15	7.8	1064.2	25	2.9	832.5	48	0.0	339.5	Total	6	14.5	1326.4	7	12.3	1323.1	14	3.4	1076.4

From Table 4, we can see that the instances become significantly more challenging when a heterogeneous fleet is allowed after electrification. For these 100 instances, BD1 produced optimal solutions to 21, while BD2 and BD3 provided optimality certificates for 32 and 62, respectively. Additionally, the highest average optimality gaps reported by BD1 are 14.2% and 22.3% for instance groups with zero and non-zero buffer times, respectively. These numbers were reduced to 8.8% and 18.7% by incorporating Pareto-optimal cuts, as shown in results delivered by BD2. Meanwhile, BD3 managed to control the average optimality gaps within 0.3% and 6.9% for instance groups with zero and non-zero buffer times, respectively. This clearly demonstrates the value of subproblem reduction. As for the computational efficiency, the impact of Pareto-optimal cuts is more profound on instances that are less computationally challenging (e.g., the first three groups in the table). In contrast, the subproblem reduction techniques provide greater acceleration effects for more challenging instances (e.g., groups $(40, 10, 0)$, $(10, 10, 5)$, and $(10, 20, 5)$).

6.3 Benefits of electrification

The second part of our numerical experiments investigated the value of electrification. In particular, we focused on the benefits brought by electrification from three metrics: (i) the reduction in fuel consumption, (ii) the reduction in fleet operating cost, and (iii) the value of incorporating buffer charging times in vehicle scheduling. To this end, we built up a simulation model using the GPS records obtained from the major Canadian seaport. Let $\mathcal{R}^0$ denote the set of routes used in the simulation model, which were generated from the GPS records. Each route represents a truck's operations in a four-hour shift. Given any electrification plan $(\boldsymbol{x}, \boldsymbol{y}) \in \mathbf{X}$, we evaluate its performance through running the simulation model for a set of shifts $\mathcal{S}$ (we set $|\mathcal{S}| = 5,000$ in the experiments). Each shift $s \in \mathcal{S}$ covers a four-hour period. For each shift $s \in \mathcal{S}$, we randomly sample a subset of routes $\mathcal{R}_s$ from $\mathcal{R}^0$ such that $|\mathcal{R}_s| = F$.

As shown in Table 4 and discussed in EC.4 of the electronic companion, allowing fleet heterogeneity in electrification (i.e., $\Gamma = 0$) yields only marginal benefits while significantly increasing computational complexity. Therefore, when evaluating the value of electrification, we restricted our computational experiments to instances with fleet homogeneity ($\Gamma = 1$). Given $\Gamma = 1$, $\delta \in \{0\%, 5\%\}$, $F \in \{10, 20, 30, 40, 50\}$, and $|\mathcal{R}| \in \{10, 20, 40, 50\}$, there are 40 parameter combinations. For each combination, we generated an instance, leading to 40 instances in total. Each instance was generated through a data-driven sampling approach for creating the route samples. Details of the sampling approach are explained in EC.4.1 of the electronic companion. Compared with random sampling, this sampling approach leads to better out-of-sample performance. We solved all instances using BD3. The approach managed to obtain optimal solutions to 36 out of the 40 instances within the time limit and maintained the optimality gaps for all instances within 1.5%.

The benefits of electrification in terms of operating cost and fuel consumption are examined through the simulation model based on the solutions obtained by BD3 on the 40 instances. To quantify such benefits, we let $C'_r(\boldsymbol{x}, \boldsymbol{y})$ (resp. $G'_r(\boldsymbol{x}, \boldsymbol{y})$) and $\overline{C}_r$ (resp. $\overline{G}_r$) denote the cost (resp. fuel consumption) of a vehicle retrofitted with configuration $h(r)$ and a diesel vehicle to run on route $r \in \mathcal{R}_s$ with $s \in \mathcal{S}$, respectively, where $h(r)$ is determined by the simulation model based on the fleet retrofitting solution $\boldsymbol{x}$. Then we calculate the out-of-sample reduction ratios (in percentage) regarding cost and fuel consumption associated with the solution as follows:

$$\sigma^{\text{cost}}(\boldsymbol{x}, \boldsymbol{y}) = 100 \left(1 - \frac{\sum_{f \in [F]^+} \sum_{h \in \mathcal{H}} C^1_h f x_{f,h} + \sum_{k \in \mathcal{K}} \sum_{v \in \mathcal{V}^1} C^2_{k,v} y_{k,v} + Q \sum_{s \in \mathcal{S}} \sum_{r \in \mathcal{R}_s} \frac{1}{|\mathcal{S}|} C'_r}{Q \sum_{s \in \mathcal{S}} \sum_{r \in \mathcal{R}_s} \frac{1}{|\mathcal{S}|} \overline{C}_r} \right),$$

$$\sigma^{\text{fuel}}(\boldsymbol{x}, \boldsymbol{y}) = 100 \left(1 - \frac{Q \sum_{s \in \mathcal{S}} \sum_{r \in \mathcal{R}_s} \frac{1}{|\mathcal{S}|} G'_r}{Q \sum_{s \in \mathcal{S}} \sum_{r \in \mathcal{R}_s} \frac{1}{|\mathcal{S}|} \overline{G}_r} \right),$$

where Q, with a slight abuse of notation, denotes the number of shifts within the planning horizon. It is worth mentioning that, in the simulation model, the impact of congestion on charging the vehicles have been factored into the calculation of $C'_r(\boldsymbol{x}, \boldsymbol{y})$ and $G'_r(\boldsymbol{x}, \boldsymbol{y})$. We found that, for container drayage in a seaport, the impact of congestion on opportunity charging is very marginal. In particular, there is no congestion for vehicle charging in the case with zero buffer times for charging, while the valid charging times are reduced by 3% on average due to congestion at charging stations in the case with non-zero buffer times for charging.

Figure 2 depicts reductions in fuel consumption and cost brought by electrification under different buffer time ratios. One can observe that the reductions in cost and fuel consumption generally increase with the fleet size and the sample size for solving the problem. A larger fleet size allows for higher utilization of charging facilities, creating better economies of scale and resulting in greater savings in operational costs in the long term. Additionally, since the electrification budget $B = 10,000 \times F$ scales with fleet size F, larger fleets provide greater planning flexibility, potentially yielding more efficient electrification decisions. Furthermore, since larger samples typically better represent real-world applications, the out-of-sample performance of a model improves with its sample size.

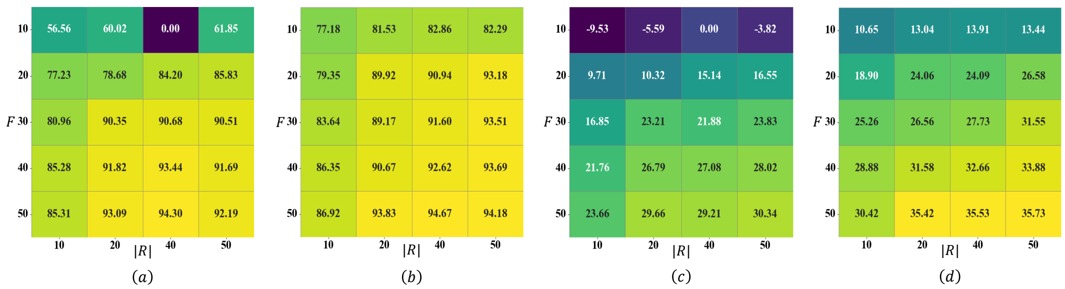

Figure 2: Fuel consumption and cost changes (in %): (a) Fuel consumption reduction under $\delta = 0\%$, (b) Fuel consumption reduction under $\delta = 5\%$, (c) Cost reduction under $\delta = 0\%$, (d) Cost reduction under $\delta = 5\%$.

The EPPOC is formulated as a cost-minimization problem, and the non-electrification solution (i.e., deploying no charging stations and operating all vehicles in diesel mode) is a feasible solution to the problem. Therefore, charging stations will be deployed and vehicles will be electrified only when such decisions lead to cost reductions compared with the non-electrification solution. This explains the zero cost and fuel consumption reductions in an instance, as the model identifies non-electrification as the most cost-effective solution. However, we observe that there were also negative cost reduction ratios in the simulation. This is due to the divergence between the in-sample and out-of-sample performance of a solution.

Finally, regarding the value of allocating buffer times for vehicle charging, the comparisons between Figures 2(a) and 2(b) and between 2(c) and 2(d) attest to the substantial extra value added by the charging buffers and indicate that such add-on value is even more significant when the fleet size is relatively small.

7 Conclusions

In this paper, we have introduced an EPPOC faced by HDV operators that addresses fleet retrofitting and charging station deployment decisions in combination. We have formulated the problem as a compact MILP model and developed a solution approach based on Benders decomposition. Several important computational enhancements have been proposed for improving the algorithm, including a series of novel subproblem reduction techniques. We have proved the validity of subproblem reduction and the strength of substitute cuts generated in this procedure. We have conducted extensive numerical experiments based on instances generated from a real electrification project to examine the performance of the solution approach. The results demonstrate that our solution approach significantly outperforms a commonly used MILP solver and that the enhancement strategies, particularly the subproblem reduction techniques, significantly improve the performance of the approach. Application-wise, the results demonstrate that electrification can cut down fuel consumption by over 90% and also contribute to significant cost savings of up to 35%.

Our study makes several important implications. For industrial practitioners, it provides an efficient solution approach to the EPPOC and shows the dual cost and environmental benefits of electrification. Further, from a computational perspective, our solution framework and enhancement strategies provide valuable computational insights for electrification planning problems that involve coordinated decision-making between fleet composition and charging facility deployment. Amid escalating global warming, and with advancements in electrification technologies, such problems are gaining ever-increasing attention from various stakeholders. The proposed subproblem reduction techniques also provide references for accelerating Benders decomposition with a large number of subproblems.

Electronic companion

EC.1 Notation for the EPPOC

Table EC.1 lists the notation used in the formulation of the EPPOC.

Table EC.1: Notation for the EPPOC.

Sets	
$\mathcal{H}$	set of potential configurations for vehicle retrofitting.
$\mathcal{V}$	set of vertices of the operation network.
$\mathcal{V}'$	set of candidate vertices for deploying charging stations; $\mathcal{V}' \subseteq \mathcal{V}$.
$\mathcal{E}$	set of edges of the operation network.
$\mathcal{K}$	set of types of charging stations.
$\mathcal{R}$	set of routes operated by the fleet.
$\mathcal{L}$	set of legs contained in all routes.
$\mathcal{L}_r$	set of legs contained in route $r \in \mathcal{R}$; $\mathcal{L}_r \subseteq \mathcal{L}$; $\mathcal{L}_{r_1} \cap \mathcal{L}_{r_2} = \varnothing$, $\forall r_1, r_2 \in \mathcal{R} : r_1 \neq r_2$.
$\mathcal{N}$	set of nodes (i.e., sequenced vertices) contained in all routes.
$\mathcal{N}_r$	set of nodes contained in route $r \in \mathcal{R}$; $\mathcal{N}_r \subseteq \mathcal{N}$; $\mathcal{N}_{r_1} \cap \mathcal{N}_{r_2} = \varnothing$, $\forall r_1, r_2 \in \mathcal{R} : r_1 \neq r_2$.
$\mathcal{N}_l$	set of nodes contained in leg $l \in \mathcal{L}$; $\mathcal{N}_l \subseteq \mathcal{N}$; $\mathcal{N}_{l_1} \cap \mathcal{N}_{l_2} = \varnothing$, $\forall l_1, l_2 \in \mathcal{R} : l_1 \neq l_2$.
$\mathcal{A}$	set of arcs contained in all routes.
$\mathcal{A}_r$	set of arcs contained in route $r \in \mathcal{R}$; $\mathcal{A}_r \subseteq \mathcal{A}$; $\mathcal{A}_{r_1} \cap \mathcal{A}_{r_2} = \varnothing$, $\forall r_1, r_2 \in \mathcal{R} : r_1 \neq r_2$.
Parameters	
F	number of vehicles in the fleet.
p_h	default charging rate of configuration $h \in \mathcal{H}$.
q_h	battery capacity of configuration $h \in \mathcal{H}$.
C^1_h	cost of retrofitting a vehicle with configuration $h \in \mathcal{H}$.
g_k	default charging speed of a type-k charging station, where $k \in \mathcal{K}$.
$C^2_{v,k}$	cost of setting up a type-k charging station at vertex $v \in \mathcal{V}$.
B	budget of electrification.
w_i	minimum dwell time of any vehicle on node $i \in \mathcal{N}$.
T_l	maximum allowable total dwell time on the nodes of leg $l \in \mathcal{L}$.
d_a	length of arc $a \in \mathcal{A}$.
b	electricity consumption for each unit distance traveled by any vehicle in electric mode.
a^0_h	initial battery charge for a vehicle with configuration $h \in \mathcal{H}$ embarking on a route.
D	unit-distance cost of any vehicle for energy consumption in diesel mode.
E	unit-distance cost of any vehicle for energy consumption in electric mode.
o_r	weight of route $r \in \mathcal{R}$ for calculating its contribution in the expected total cost within the planning horizon for electrification.
Decision Variables	
$x_{f,h}$	binary variable, which equals 1 if and only if $f \in [F]$ vehicles in the fleet are retrofitted with configuration $h \in \mathcal{H}$.
$y_{v,k}$	binary variable, which equals 1 if and only if a type-k charging station is deployed at vertex $v \in \mathcal{V}$.
$u_{h,i}$	continuous variable, representing the dwell time of any vehicle with configuration $h \in \mathcal{H}$ at node $i \in \mathcal{N}$.
$\alpha_{h,i}$	continuous variable, representing the battery charge of any vehicle with configuration $h \in \mathcal{H}$ at its arrival at node $i \in \mathcal{N}$.
$\beta_{h,i}$	continuous variable, representing the electricity recharged by any vehicle with configuration $h \in \mathcal{H}$ at node $i \in \mathcal{N}$.
$\mu_{h,a}$	continuous variable, representing the distance traversed in electric mode, by any vehicle with configuration $h \in \mathcal{H}$ on arc $a \in \mathcal{A}$.
$\nu_{h,a}$	continuous variable, representing the distance traversed in diesel mode, by any vehicle with configuration $h \in \mathcal{H}$ on arc $a \in \mathcal{A}$.
$z_{h,r}$	continuous variable, representing the energy consumption cost of any vehicle with configuration $h \in \mathcal{H}$ running on route $r \in \mathcal{R}$.
Z	continuous variable, representing the expected operational costs for running the entire fleet during the planning horizon.

EC.2 Mathematical proofs

This section presents the proofs of the theorems, propositions, and lemmas introduced in the main text.

EC.2.1 Proof of Theorem 1

Proof of Theorem 1. Given any $(\bar{\boldsymbol{x}}, \bar{\boldsymbol{y}}) \in \mathbf{X}$, $h \in \mathcal{H}$, and $r \in \mathcal{R}$, the primal and dual subproblems $\mathrm{PSP}_{h,r}(\bar{\boldsymbol{x}}, \bar{\boldsymbol{y}})$ and $\mathrm{DSP}_{h,r}(\bar{\boldsymbol{x}}, \bar{\boldsymbol{y}})$ are both linear programs. Hence, strong duality holds between them. Therefore, it is sufficient to show that the primal problem $\mathrm{PSP}_{h,r}(\bar{\boldsymbol{x}}, \bar{\boldsymbol{y}})$ is feasible and bounded.

To show its feasibility, consider the following solution $\mathbf{S} = \{\boldsymbol{u}, \boldsymbol{\alpha}, \boldsymbol{\beta}, \boldsymbol{\gamma}, \boldsymbol{\mu}, \boldsymbol{\nu}\}$ to $\mathrm{PSP}_{h,r}(\bar{\boldsymbol{x}}, \bar{\boldsymbol{y}})$:

$$u_{h,i} = w_i \qquad \forall i \in \mathcal{N}_r \tag{EC.1}$$
$$\alpha_{h,i} = \alpha_h^0 \qquad \forall i \in \mathcal{N}_r \tag{EC.2}$$
$$\nu_{h,a} = d_a \qquad \forall a \in \mathcal{A}_r \tag{EC.3}$$
$$\beta_{h,i}, \gamma_{h,k,i}, \mu_{h,a} = 0 \qquad \forall a \in \mathcal{A}_r, i \in \mathcal{N}_r, k \in \mathcal{K}. \tag{EC.4}$$

It is easy to verify that $\mathbf{S}$ is a feasible solution to $\mathrm{PSP}_{h,r}(\bar{\boldsymbol{x}}, \bar{\boldsymbol{y}})$, which attests to the feasibility of the problem. Further, as $\mu_{h,a} \geq 0$ and $\nu_{h,a} \geq 0$, we have $E\sum_{a\in\mathcal{A}_r} \mu_{h,a} + D\sum_{a\in\mathcal{A}_r} \nu_{h,a} \geq 0$. Hence, $\mathrm{PSP}_{h,r}(\bar{\boldsymbol{x}}, \bar{\boldsymbol{y}})$ is also bounded. This completes the proof. □

EC.2.2 Proof of Proposition 1

We use the procedure depicted in Algorithm EC.1 for generating a solution to any $\mathrm{DSP}_{h,r}(\bar{\boldsymbol{x}}, \bar{\boldsymbol{y}})$ with $\sum_{i\in\mathcal{N}_l} w_i = T_l$ in $\mathcal{O}(|\mathcal{N}_r||\mathcal{K}|)$ time, where $(\bar{\boldsymbol{x}}, \bar{\boldsymbol{y}}) \in \mathbf{X}$, $h \in \mathcal{H}$, and $r \in \mathcal{R}$.

Proof of Proposition 1. It is sufficient to show that algorithm EC.1 obtains an optimal solution to $\mathrm{DSP}_{h,r}(\bar{\boldsymbol{x}}, \bar{\boldsymbol{y}})$ with $\sum_{i\in\mathcal{N}_l} w_i = T_l$, where $h \in \mathcal{H}$ and $r \in \mathcal{R}$.

Since $D > E$, any optimal solution to the primal subproblem $\mathrm{PSP}_{h,r}(\bar{\boldsymbol{x}}, \bar{\boldsymbol{y}})$ maximizes the total distance of the vehicle traveling in electric mode (i.e., $\sum_{a\in\mathcal{A}_r} \mu_{h,a}$). Following this, we construct an optimal solution to the $\mathrm{PSP}_{h,r}(\bar{\boldsymbol{x}}, \bar{\boldsymbol{y}})$ that maximizes the electricity that can be charged by the vehicle on the route.

As strong duality exists between the primal subproblem $\mathrm{PSP}_{h,r}(\bar{\boldsymbol{x}}, \bar{\boldsymbol{y}})$ and its dual subproblem $\mathrm{DSP}_{h,r}(\bar{\boldsymbol{x}}, \bar{\boldsymbol{y}})$, the optimal solution to the primal directly facilitates the construction of an optimal solution to the dual. Using the Karush-Kuhn-Tucker (KKT) conditions, Algorithm EC.1 achieves this by appropriately setting the values of the decision variables associated with the nodes in route r in reverse order. □

EC.2.3 Proof of Proposition 2

Proof of Proposition 2. Given any route $r \in \mathcal{R}$ and configuration $h \in \mathcal{H}$, let $z^*_{h,r}(\bar{\boldsymbol{x}}, \bar{\boldsymbol{y}})$ be the optimal objective function value to $\mathrm{PSP}_{h,r}(\bar{\boldsymbol{x}}, \bar{\boldsymbol{y}})$, for any MP solution $(\bar{\boldsymbol{x}}, \bar{\boldsymbol{y}}) \in \mathbf{X}$. To show the validity of inequalities (30) and (31), it is sufficient to prove the following two inequalities hold:

$$z^*_{h,r}(\bar{\boldsymbol{x}}, \bar{\boldsymbol{y}}) \geq E \sum_{a\in\mathcal{A}_r} d_a, \tag{EC.5}$$
$$z^*_{h,r}(\bar{\boldsymbol{x}}, \bar{\boldsymbol{y}}) \geq D \sum_{a\in\mathcal{A}_r} d_a - (\alpha_h^0 + \sum_{i\in\mathcal{N}_r} \sum_{k\in\mathcal{K}} \bar{y}_{k,v(i)} M^1_{h,k,i})/b(D-E). \tag{EC.6}$$

Algorithm EC.1 Solution algorithm for the DSP$_{h,r}(\bar{\boldsymbol{x}}, \bar{\boldsymbol{y}})$ with $\sum_{i\in\mathcal{N}_l} w_i = T_l$.

/*Solve the primal subproblem*/
Initialize: set the initial battery charge $\alpha_{h,i(r,1)} \leftarrow \alpha_h^0$
for $n = 1, ..., |\mathcal{N}_r| - 1$ **do**
    Update: Node: $i \leftarrow i(r,n)$; Arc: $a \leftarrow a(r,n)$; Vertex: $v \leftarrow v(i)$; Electricity charged: $\beta_{h,i} \leftarrow 0$
    $\beta_{h,i} \leftarrow \min\{(\sum_{k\in\mathcal{K}} x_{k,v} w_i g_k), (w_i p_h), (q_h - \alpha_{h,i})\}$; $\mu_{h,a} \leftarrow \min\{d_a, \frac{(\alpha_{h,i}+\beta_{h,i})}{b}\}$; $\nu_{h,a} \leftarrow d_a - \mu_{h,a}$; $\alpha_{h,i+1} \leftarrow \alpha_{h,i} + \beta_{h,i} - b\mu_{h,a}$
end for
$\beta_{h,|\mathcal{N}_r|} \leftarrow 0$
/*Solve the dual subproblem*/
$\phi_{|\mathcal{N}_r|} \leftarrow 0$; $\psi_{|\mathcal{N}_r|} \leftarrow 0$; $\varphi_{|\mathcal{N}_r|} \leftarrow 0$
if $\alpha_{h,|\mathcal{N}_r|} > 0$ **then**
    $\pi_{|\mathcal{N}_r|-1} \leftarrow 0$; $\vartheta_{a(r,|\mathcal{N}_r|-1)} \leftarrow E$
else
    $\pi_{|\mathcal{N}_r|-1} \leftarrow E - \frac{D}{b}$; $\vartheta_{a(r,|\mathcal{N}_r|-1)} \leftarrow D$
end if
for $n = |\mathcal{N}_r| - 1, ..., 1$ **do**
    Update: Node: $i \leftarrow i(r,n)$; Arc: $a \leftarrow a(r,n)$; Vertex: $v \leftarrow v(i)$; Electricity charged: $\beta_{h,i} \leftarrow 0$
    if $\beta_{h,i} = \sum_{k\in\mathcal{K}} x_{k,v} w_i g_k$ **then**
        $\phi_{h,i} \leftarrow \pi_n$; $\psi_{h,i} \leftarrow 0$; $\varphi_{h,i} \leftarrow 0$
    end if
    if $\beta_{h,i} \neq \sum_{k\in\mathcal{K}} x_{k,v} w_i g_k$ & $\beta_{h,i} = q_h - \alpha_{h,i}$ **then**
        $\phi_{h,i} \leftarrow 0$; $\psi_{h,i} \leftarrow \pi_n$; $\varphi_{h,i} \leftarrow 0$
    end if
    if $\beta_{h,i} \neq \sum_{k\in\mathcal{K}} x_{k,v} w_i g_k$ & $\beta_{h,i} \neq q_h - \alpha_{h,i}$ & $\beta_{h,i} = w_i p_h$ **then**
        $\phi_{h,i} \leftarrow 0$; $\psi_{h,i} \leftarrow 0$; $\varphi_{h,i} \leftarrow \pi_n$
    end if
    if $n \geq 2$ **then**
        if $\alpha_{h,i} > 0$ **then**
            $\pi_{n-1} \leftarrow \pi_n - \phi_{h,i}$; $\vartheta_{a(r,n-1)} \leftarrow E - b\pi_{n-1}$;
        else
            $\pi_{n-1} \leftarrow \frac{E-D}{b}$; $\vartheta_{a(r,n-1)} \leftarrow D$
        end if
    end if
end for

Let $\boldsymbol{\mu}^*$, $\boldsymbol{\nu}^*$, $\boldsymbol{\alpha}^*$, and $\boldsymbol{\beta}^*$ denote the vectors for the values of $\mu_{h,a}$, $\nu_{h,a}$, $\alpha_{h,i}$, $\beta_{h,i}$ variables ($i \in \mathcal{N}_r$, $a \in \mathcal{A}_r$) in an optimal solution to PSP$_{h,r}(\bar{\boldsymbol{x}}, \bar{\boldsymbol{y}})$, then we have:

$$z^*_{h,r}(\bar{\boldsymbol{x}}, \bar{\boldsymbol{y}}) = E \sum_{a\in\mathcal{A}_r} \mu^*_{h,a} + D \sum_{a\in\mathcal{A}_r} \nu^*_{h,a}. \tag{EC.7}$$

Due to constraints (26d), Equation (EC.7) is equivalent to $z^*_{h,r}(\bar{\boldsymbol{x}}, \bar{\boldsymbol{y}}) = E\sum_{a\in\mathcal{A}_r} d_a + (D - E)\sum_{a\in\mathcal{A}_r} \nu^*_{h,a}$. As $D > E$ and $\nu^*_{h,a} \geq 0$, $\forall a \in \mathcal{A}_r$, we have $z^*_{h,r}(\bar{\boldsymbol{x}}, \bar{\boldsymbol{y}}) \geq E\sum_{a\in\mathcal{A}_r} d_a$, indicating that (EC.5) is valid. In addition, considering constraints (26d), we can also write $z^*_{h,r}(\bar{\boldsymbol{x}}, \bar{\boldsymbol{y}})$ as

$$z^*_{h,r}(\bar{\boldsymbol{x}}, \bar{\boldsymbol{y}}) = D \sum_{a\in\mathcal{A}_r} d_a - (D - E) \sum_{a\in\mathcal{A}_r} \mu^*_{h,a}. \tag{EC.8}$$

Then due to constraints (26g), we have

$$\sum_{a\in\mathcal{A}_r} \mu^*_{h,a} = \sum_{n\in[N_r-1]^+} (\alpha^*_{h,i(r,n)} + \beta^*_{h,i(r,n)} - \alpha^*_{h,i(r,n+1)})/b,$$

which is equivalent to

$$\sum_{a\in\mathcal{A}_r} \mu^*_{h,a} = (\alpha^*_{h,i(r,1)} + \sum_{n\in[N_r-1]^+} \beta^*_{h,i(r,n)})/b. \tag{EC.9}$$

From constraints (26i) and (26j), we have $\beta^*_{h,i} \leq \sum_{k\in\mathcal{K}} \bar{y}_{k,v(i)} M^1_{h,k,i}$, $\forall i \in \mathcal{N}_r$, which, in combination with (26e) and (EC.9) gives

$$\sum_{a\in\mathcal{A}_r} \mu^*_{h,a} \leq (\alpha^0_h + \sum_{i\in\mathcal{N}_r}\sum_{k\in\mathcal{K}} \bar{y}_{k,v(i)} M^1_{h,k,i})/b. \tag{EC.10}$$

Combining (EC.8) and (EC.10) gives (EC.6). This completes the proof. □

EC.2.4 Proof of Lemma 1

Proof of Lemma 1. $\mathrm{DSP}_{h,r}(\bar{\boldsymbol{x}}^1, \bar{\boldsymbol{y}}^1)$ and $\mathrm{DSP}_{h,r}(\bar{\boldsymbol{x}}^2, \bar{\boldsymbol{y}}^2)$ are defined on the identical set of constraints (i.e., (27b)–(27l)). Further, given any $h \in \mathcal{H}$ and $r \in \mathcal{R}$ and two MP solutions $(\bar{\boldsymbol{x}}^1, \bar{\boldsymbol{y}}^1), (\bar{\boldsymbol{x}}^2, \bar{\boldsymbol{y}}^2) \in \mathbf{X}$, suppose that conditions (i) and (ii) hold, then we have

$$M^1_{h,k,i}\bar{y}^1_{k,v(i)} = M^1_{h,k,i}\bar{y}^2_{k,v(i)}, \qquad \forall k \in \mathcal{K}, i \in \mathcal{N}_r.$$

This is sufficient to show that $\mathrm{DSP}_{h,r}(\bar{\boldsymbol{x}}^1, \bar{\boldsymbol{y}}^1)$ is equivalent to $\mathrm{DSP}_{h,r}(\bar{\boldsymbol{x}}^2, \bar{\boldsymbol{y}}^2)$, which further indicates that $\zeta_{h,r}(\bar{\boldsymbol{x}}^1, \bar{\boldsymbol{y}}^1) = \zeta_{h,r}(\bar{\boldsymbol{x}}^2, \bar{\boldsymbol{y}}^2)$. □

EC.2.5 Proof of Proposition 3

Proof of Proposition 3. Given any $h \in \mathcal{H}$ and $r \in \mathcal{R}$, a MP solution $(\bar{\boldsymbol{x}}^2, \bar{\boldsymbol{y}}^2) \in \mathbf{X}$, and a core point $(\boldsymbol{x}^c, \boldsymbol{y}^c)$, from the proof of Lemma 1, we have that the following constraint in $\text{PO-DSP}_{h,r}(\bar{\boldsymbol{x}}^2, \bar{\boldsymbol{y}}^2, \zeta^2_{h,r}, \boldsymbol{x}^c, \boldsymbol{y}^c)$:

$$\sum_{i\in\mathcal{N}_r} w_i\eta_i + \sum_{l\in\mathcal{L}_r} T_l\theta_l + \sum_{a\in\mathcal{A}_r} d_a\vartheta_a + \alpha^0_h\kappa + \sum_{i\in\mathcal{N}_r} q_h\psi_i + \sum_{k\in\mathcal{K}}\sum_{i\in\mathcal{N}_r} M^1_{h,k,i}\varrho_{i,k}\bar{y}_{k,v(i)} = \zeta^2_{h,r}$$

is equivalent to

$$\sum_{i\in\mathcal{N}_r} w_i\eta_i + \sum_{l\in\mathcal{L}_r} T_l\theta_l + \sum_{a\in\mathcal{A}_r} d_a\vartheta_a + \alpha^0_h\kappa + \sum_{i\in\mathcal{N}_r} q_h\psi_i + \sum_{k\in\mathcal{K}}\sum_{i\in\mathcal{N}_r} M^1_{h,k,i}\varrho_{i,k}\bar{y}_{k,v(i)} = \zeta^1_{h,r}.$$

Therefore, similar to the proof of Lemma 1, we have $\text{PO-DSP}_{h,r}(\bar{\boldsymbol{x}}^1, \bar{\boldsymbol{y}}^1, \zeta^1_{h,r}, \boldsymbol{x}^c, \boldsymbol{y}^c)$ is equivalent to $\text{PO-DSP}_{h,r}(\bar{\boldsymbol{x}}^2, \bar{\boldsymbol{y}}^2, \zeta^2_{h,r}, \boldsymbol{x}^c, \boldsymbol{y}^c)$, and their optimal solutions are shared. □

EC.2.6 Proof of Corollary 1

Proof of Corollary 1. The corollary is a direct result of Proposition 3. □

EC.2.7 Proof of Lemma 2

Proof of Lemma 2. Given any MP solution $(\bar{\boldsymbol{x}}, \bar{\boldsymbol{y}}) \in \mathbf{X}$, for a specific route $r \in \mathcal{R}$, suppose that we have two configurations $h_1, h_2 \in \mathcal{H}$ that satisfy conditions (i)$-$(iii), then one can easily verify that any feasible solution to the primal subproblem $\mathrm{PSP}_{h_1,r}(\bar{\boldsymbol{x}}, \bar{\boldsymbol{y}})$ is also a feasible solution to $\mathrm{PSP}_{h_2,r}(\bar{\boldsymbol{x}}, \bar{\boldsymbol{y}})$ and vice versa. In addition, $\mathrm{PSP}_{h_1,r}(\bar{\boldsymbol{x}}, \bar{\boldsymbol{y}})$ and $\mathrm{PSP}_{h_2,r}(\bar{\boldsymbol{x}}, \bar{\boldsymbol{y}})$ have identical objective functions. Therefore, they also have the same optimal objective function values. Since strong duality holds for $\mathrm{PSP}_{h,r}(\bar{\boldsymbol{x}}, \bar{\boldsymbol{y}})$ and $\mathrm{DSP}_{h,r}(\bar{\boldsymbol{x}}, \bar{\boldsymbol{y}})$, $\forall h \in \mathcal{H}, r \in \mathcal{R}$, we have $\zeta_{h_1,r}(\bar{\boldsymbol{x}}, \bar{\boldsymbol{y}}) = \zeta_{h_2,r}(\bar{\boldsymbol{x}}, \bar{\boldsymbol{y}})$. □

EC.2.8 Proof of Proposition 4

Proof of Proposition 4. To begin with, we have $\bar{\boldsymbol{\chi}}_{h_1,r}$ is feasible for constraints (27c)–(27l) in PO-DSP$_{h_2,r}(\bar{\boldsymbol{x}}, \bar{\boldsymbol{y}}, \zeta_{h_2,r}, \boldsymbol{x}^c, \boldsymbol{y}^c)$, since these constraints are identical for PO-DSP$_{h_1,r}(\bar{\boldsymbol{x}}, \bar{\boldsymbol{y}}, \zeta_{h_1,r}, \boldsymbol{x}^c, \boldsymbol{y}^c)$ and PO-DSP$_{h_2,r}(\bar{\boldsymbol{x}}, \bar{\boldsymbol{y}}, \zeta_{h_2,r}, \boldsymbol{x}^c, \boldsymbol{y}^c)$. Besides, we have

$$\begin{aligned}
0 &\geq \bar{\eta}_i + \bar{\theta}_l - \sum_{k\in\mathcal{K}} g_k \bar{\rho}_{i,k} - p_{h_1}\bar{\varphi}_i \\
&\geq \bar{\eta}_i + \bar{\theta}_l - \sum_{k\in\mathcal{K}} g_k \bar{\rho}_{i,k} - p_{h_2}\bar{\varphi}_i, \qquad \forall i \in \mathcal{N}_l, l \in \mathcal{L}_r,
\end{aligned}$$

where the first inequality comes from the feasibility of $\bar{\boldsymbol{\chi}}_{h_1,r}$ to PO-DSP$_{h_1,r}(\bar{\boldsymbol{x}}, \bar{\boldsymbol{y}}, \zeta_{h_1,r}, \boldsymbol{x}^c, \boldsymbol{y}^c)$ and the second inequality is a result condition (iv). Therefore, the solution is also feasible for constraints (27b).

In addition, from condition (iii), we have

$$M^1_{h_1,k,i}\bar{y}_{k,v(i)} = M^1_{h_2,k,i}\bar{y}_{k,v(i)}, \qquad \forall k \in \mathcal{K}, i \in \mathcal{N}_r. \tag{EC.11}$$

From condition (i), Lemma 2, and (EC.11), it can be deduced that constraints (29b) are also identical for the two problems. Therefore, the solution is feasible to PO-DSP$_{h_2,r}(\bar{\boldsymbol{x}}, \bar{\boldsymbol{y}}, \zeta_{h_2,r}, \boldsymbol{x}^c, \boldsymbol{y}^c)$. □

EC.2.9 Proof of Corollary 2

Proof of Corollary 2. The corollary is a direct result of Proposition 4. □

EC.2.10 Proof of Lemma 3

Proof of Lemma 3. From the KKT conditions for convex problems (Boyd and Vandenberghe 2004), there must exist an optimal solution denoted by $\boldsymbol{\chi}^*_{h,r}$ to the dual subproblem DSP$_{h,r}(\bar{\boldsymbol{x}}, \bar{\boldsymbol{y}})$ in which $\boldsymbol{\psi}^*_{h,r} = \mathbf{0}$. This solution is also feasible for the PO-DSP$_{h,r}(\bar{\boldsymbol{x}}, \bar{\boldsymbol{y}}, \zeta_{h_1,r}, \boldsymbol{x}^c, \boldsymbol{y}^c)$. □

EC.2.11 Proof of Lemma 4

Proof of Lemma 4. Consider the following problem denoted by PSP$'_{h,r}(\bar{\boldsymbol{x}}, \bar{\boldsymbol{y}})$, $\forall h \in \mathcal{H}$, $r \in \mathcal{R}$:

$$\begin{aligned}
\min_{[PSP'_{h,r}(\bar{\boldsymbol{x}}, \bar{\boldsymbol{y}})]} \quad & E\sum_{a\in\mathcal{A}_r}\mu_{h,a} + D\sum_{a\in\mathcal{A}_r}\nu_{h,a} \\
\text{s.t.} \quad & (26b) - (26h), (26j), (26l), \text{ and,} \\
& \gamma_{h,k,i} \leq g_k \bar{t}_i \bar{y}_{k,v(i)} \quad \forall i \in \mathcal{N}_r, k \in \mathcal{K}.
\end{aligned}$$

Let $\zeta'_{h_1,r}(\bar{\boldsymbol{x}}, \bar{\boldsymbol{y}})$ and $\zeta'_{h_2,r}(\bar{\boldsymbol{x}}, \bar{\boldsymbol{y}})$ denote the optimal solutions to PSP$'_{h_1,r}(\bar{\boldsymbol{x}}, \bar{\boldsymbol{y}})$ and PSP$'_{h_2,r}(\bar{\boldsymbol{x}}, \bar{\boldsymbol{y}})$, respectively. From condition (iv), we have

$$\begin{aligned}
\zeta'_{h_1,r}(\bar{\boldsymbol{x}}, \bar{\boldsymbol{y}}) &= \zeta_{h_1,r}(\bar{\boldsymbol{x}}, \bar{\boldsymbol{y}}), \\
\zeta'_{h_2,r}(\bar{\boldsymbol{x}}, \bar{\boldsymbol{y}}) &= \zeta_{h_2,r}(\bar{\boldsymbol{x}}, \bar{\boldsymbol{y}}).
\end{aligned}$$

Let $(\boldsymbol{u}^*_{h_1,r}, \boldsymbol{\alpha}^*_{h_1,r}, \boldsymbol{\beta}^*_{h_1,r}, \boldsymbol{\gamma}^*_{h_1,r}, \boldsymbol{\mu}^*_{h_1,r}, \boldsymbol{\nu}^*_{h_1,r})$ denote an optimal solution to PSP$'_{h_1,r}(\bar{\boldsymbol{x}}, \bar{\boldsymbol{y}})$, such that (32) holds. Conditions (ii) and (iii) indicate that $(\boldsymbol{u}^*_{h_1,r}, \boldsymbol{\alpha}^*_{h_1,r}, \boldsymbol{\beta}^*_{h_1,r}, \boldsymbol{\gamma}^*_{h_1,r}, \boldsymbol{\mu}^*_{h_1,r}, \boldsymbol{\nu}^*_{h_1,r})$ is a feasible solution to PSP$'_{h_2,r}(\bar{\boldsymbol{x}}, \bar{\boldsymbol{y}})$. Therefore, we have $\zeta'_{h_2,r}(\bar{\boldsymbol{x}}, \bar{\boldsymbol{y}}) \leq \zeta'_{h_1,r}(\bar{\boldsymbol{x}}, \bar{\boldsymbol{y}})$, which indicates

$$\zeta_{h_2,r}(\bar{\boldsymbol{x}}, \bar{\boldsymbol{y}}) \leq \zeta_{h_1,r}(\bar{\boldsymbol{x}}, \bar{\boldsymbol{y}}). \tag{EC.12}$$

Given any $h \in \mathcal{H}$ and $r \in \mathcal{R}$, let $\text{DSP}'_{h,r}(\bar{\boldsymbol{x}}, \bar{\boldsymbol{y}})$ be the dual of $\text{PSP}'_{h,r}(\bar{\boldsymbol{x}}, \bar{\boldsymbol{y}})$, which can be formulated as:

$$\max_{[\text{DSP}'_{h,r}(\bar{\boldsymbol{x}}, \bar{\boldsymbol{y}})]} \quad \sum_{i\in\mathcal{N}_r} w_i\eta_i + \sum_{l\in\mathcal{L}_r} T_l\theta_l + \sum_{a\in\mathcal{A}_r} d_a\vartheta_a + \alpha_h^0\kappa + \sum_{i\in\mathcal{N}_r} q_h\psi_i + \sum_{k\in\mathcal{K}}\sum_{i\in\mathcal{N}_r} g_k\bar{t}_i\bar{y}_{k,v(i)}\varrho_{i,k} \tag{EC.13a}$$

s.t. (27c) – (27g), (27j), (27k) and,

$$\eta_i + \theta_l - \sum_{k\in\mathcal{K}} g_k\rho_{i,k} \le 0 \quad \forall i \in \mathcal{N}_l, l \in \mathcal{L}_r, \tag{EC.13b}$$

$$\psi_{i(r,n)} - \pi_n + \phi_{i(r,n)} \le 0 \quad \forall n \in [N_r - 1]^+, \tag{EC.13c}$$

$$\psi_{i(r,N_r)} + \phi_{i(r,N_r)} \le 0, \tag{EC.13d}$$

$$\theta_l, \psi_i, \rho_{i,k}, \varrho_{i,k}, \phi_i \le 0 \quad \forall i \in \mathcal{N}_r, a \in \mathcal{A}_r, l \in \mathcal{L}_r, k \in \mathcal{K}. \tag{EC.13e}$$

From KKT conditions, there must be an optimal solution to $\text{DSP}'_{h_1,r}(\bar{\boldsymbol{x}}, \bar{\boldsymbol{y}})$, denoted by $\boldsymbol{\chi}^*_{h_1,r}$, in which $\boldsymbol{\psi}^*_{h_1,r} = \mathbf{0}$. It follows that $\sum_{i\in\mathcal{N}_r} w_i\eta^*_{h_1,r,i} + \sum_{l\in\mathcal{L}_r} T_l\theta^*_{h_1,r,l} + \sum_{a\in\mathcal{A}_r} d_a\vartheta^*_{h_1,r,a} + \alpha^0_{h_1}\kappa^*_{h_1,r} + \sum_{k\in\mathcal{K}}\sum_{i\in\mathcal{N}_r} g_k\bar{t}_i\bar{y}_{k,v(i)}\varrho^*_{h_1,i,k} = \zeta'_{h_1,r}(\bar{\boldsymbol{x}}, \bar{\boldsymbol{y}})$.

One can easily verify that $\boldsymbol{\chi}^*_{h_1,r}$ is an feasible solution to $\text{DSP}'_{h_2,r}(\bar{\boldsymbol{x}}, \bar{\boldsymbol{y}})$. This indicates that $\zeta'_{h_2,r}(\bar{\boldsymbol{x}}, \bar{\boldsymbol{y}}) \ge \sum_{i\in\mathcal{N}_r} w_i\eta^*_{h_1,r,i} + \sum_{l\in\mathcal{L}_r} T_l\theta^*_{h_1,r,l} + \sum_{a\in\mathcal{A}_r} d_a\vartheta^*_{h_1,r,a} + \alpha^0_{h_2}\kappa^*_{h_1,r} + \sum_{k\in\mathcal{K}}\sum_{i\in\mathcal{N}_r} g_k\bar{t}_i\bar{y}_{k,v(i)}\varrho^*_{h_1,i,k} = \zeta'_{h_1,r}(\bar{\boldsymbol{x}}, \bar{\boldsymbol{y}})$, where the equation is a result of condition (ii). Therefore,

$$\zeta_{h_2,r}(\bar{\boldsymbol{x}}, \bar{\boldsymbol{y}}) \ge \zeta_{h_1,r}(\bar{\boldsymbol{x}}, \bar{\boldsymbol{y}}). \tag{EC.14}$$

Combining (EC.12) and (EC.14), we have $\zeta_{h_2,r}(\bar{\boldsymbol{x}}, \bar{\boldsymbol{y}}) = \zeta_{h_1,r}(\bar{\boldsymbol{x}}, \bar{\boldsymbol{y}})$, which completes the proof. □

EC.2.12 Proof of Proposition 5

Proof. Proof of Proposition 5. Given Lemmas 3 and 4, the proof is similar to that of Proposition 4 and thus is omitted here. □

EC.2.13 Proof of Corollary 3

Proof of Corollary 3. The corollary is a direct result of Proposition 5. □

EC.2.14 Proof of Proposition 6

Proof of Proposition 6. Given $p_{h_1} = p_{h_2}$, if we further have $q_{h_1} = q_{h_2}$, then from Lemma 4, $\text{PO-DSP}_{h_2,r}(\bar{\boldsymbol{x}}, \bar{\boldsymbol{y}}, \zeta_{h_2,r}, \boldsymbol{x}^c, \boldsymbol{y}^c)$ is equivalent to $\text{PO-DSP}_{h_1,r}(\bar{\boldsymbol{x}}, \bar{\boldsymbol{y}}, \zeta_{h_1,r}, \boldsymbol{x}^c, \boldsymbol{y}^c)$. Hence, the proposition holds under $q_{h_1} = q_{h_2}$.

To prove the proposition, we have to show that it also holds under the condition $q_{h_1} < q_{h_2}$. To this end, we first show that in any optimal solution to $\text{DSP}_{h_2,r}(\bar{\boldsymbol{x}}, \bar{\boldsymbol{y}})$, denoted by $\boldsymbol{\chi}^*_{h_2,r}$, we must have $\boldsymbol{\psi}^*_{h_2,r} = \mathbf{0}$. This is achieved by contradiction.

Suppose that there exist a $\psi^*_i < 0$ in an optimal solution to $\text{DSP}_{h_2,r}(\bar{\boldsymbol{x}}, \bar{\boldsymbol{y}})$. Since $p_{h_1} = p_{h_2}$, $\text{DSP}_{h_1,r}(\bar{\boldsymbol{x}}, \bar{\boldsymbol{y}})$ and $\text{DSP}_{h_2,r}(\bar{\boldsymbol{x}}, \bar{\boldsymbol{y}})$ share the same feasible region defined by constraints (27b)–(27l). Hence, $\boldsymbol{\chi}^*_{h_2,r}$ is also feasible to $\text{DSP}_{h_1,r}(\bar{\boldsymbol{x}}, \bar{\boldsymbol{y}})$. Therefore, for its optimal objective value $\zeta_{h_1,r}(\bar{\boldsymbol{x}}, \bar{\boldsymbol{y}})$, we have

$$\begin{aligned}\zeta_{h_1,r}(\bar{\boldsymbol{x}}, \bar{\boldsymbol{y}}) &\ge \sum_{i\in\mathcal{N}_r} w_i\eta^*_i + \sum_{l\in\mathcal{L}_r} T_l\theta^*_l + \sum_{a\in\mathcal{A}_r} d_a\vartheta^*_a + \alpha^0_h\kappa^* + \sum_{i\in\mathcal{N}_r} q_{h_1}\psi^*_i + \sum_{k\in\mathcal{K}}\sum_{i\in\mathcal{N}_r} M_{h_1,k,i}\varrho^*_{i,k}y_{k,v(i)} \\ &> \sum_{i\in\mathcal{N}_r} w_i\eta^*_i + \sum_{l\in\mathcal{L}_r} T_l\theta^*_l + \sum_{a\in\mathcal{A}_r} d_a\vartheta^*_a + \alpha^0_h\kappa^* + \sum_{i\in\mathcal{N}_r} q_{h_2}\psi^*_i + \sum_{k\in\mathcal{K}}\sum_{i\in\mathcal{N}_r} M_{h_1,k,i}\varrho^*_{i,k}y_{k,v(i)},\end{aligned} \tag{EC.15}$$

where the strict inequality is a result of $q_{h_1} < q_{h_2}$ and the existence of a $\psi_i^* < 0$. From (EC.15), we further have $\zeta_{h_1,r}(\bar{\boldsymbol{x}}, \bar{\boldsymbol{y}}) > \zeta_{h_2,r}(\bar{\boldsymbol{x}}, \bar{\boldsymbol{y}})$, which forms a contradiction to Lemma 4. Therefore, one must have $\boldsymbol{\psi}^*_{h_2,r} = \mathbf{0}$ in any optimal solution to $\text{DSP}_{h_2,r}(\bar{\boldsymbol{x}}, \bar{\boldsymbol{y}})$.

Consequently, for any feasible solution to $\text{PO-DSP}_{h_2,r}(\bar{\boldsymbol{x}}, \bar{\boldsymbol{y}}, \zeta_{h_2,r}, \boldsymbol{x}^c, \boldsymbol{y}^c)$, we must also have $\boldsymbol{\psi}_{h_2,r} = \mathbf{0}$. Under $\boldsymbol{\psi}_{h_2,r} = \mathbf{0}$, $\text{PO-DSP}_{h_2,r}(\bar{\boldsymbol{x}}, \bar{\boldsymbol{y}}, \zeta_{h_2,r}, \boldsymbol{x}^c, \boldsymbol{y}^c)$ become equivalent to $\text{PO-DSP}_{h_1,r}(\bar{\boldsymbol{x}}, \bar{\boldsymbol{y}}, \zeta_{h_1,r}, \boldsymbol{x}^c, \boldsymbol{y}^c)$ with $\boldsymbol{\psi}_{h_1,r} = \mathbf{0}$. Hence, any optimal solution to $\text{PO-DSP}_{h_1,r}(\bar{\boldsymbol{x}}, \bar{\boldsymbol{y}}, \zeta_{h_1,r}, \boldsymbol{x}^c, \boldsymbol{y}^c)$ with $\boldsymbol{\psi}_{h_1,r} = \mathbf{0}$ is also an optimal solution to $\text{PO-DSP}_{h_2,r}(\bar{\boldsymbol{x}}, \bar{\boldsymbol{y}}, \zeta_{h_2,r}, \boldsymbol{x}^c, \boldsymbol{y}^c)$. This completes the proof. □

EC.3 Algorithmic details

This section presents the details for algorithms in the main text.

EC.3.1 The basic Benders decomposition algorithm

The Benders decomposition algorithm for solving the MP takes an iterative framework. We use $\mathbf{P}^0(\Lambda_{h,r}) \subseteq \mathbf{P}(\Lambda_{h,r})$ and $\mathbf{P}^m(\Lambda_{h,r}) \subseteq \mathbf{P}(\Lambda_{h,r})$ to respectively denote the initial set of Benders cuts and the set of Benders cuts in iteration m, where $h \in \mathcal{H}$ and $r \in \mathcal{R}$.

In each iteration m, we solve the MP with the Benders cuts in $\mathbf{P}^m(\Lambda_{h,r})$, where $h \in \mathcal{H}$ and $r \in \mathcal{R}$. Let vectors $\bar{\boldsymbol{x}}^m$, $\bar{\boldsymbol{y}}^m$ and $\bar{\boldsymbol{z}}^m$ denote the solution to $x_{f,h}$, $y_{v,k}$, and $z_{h,r}$ variables, respectively. Additionally, we let $\bar{\boldsymbol{\chi}}^m_{h,r}$ and $\zeta^m_{h,r}$ denote the optimal solutions to dual subproblems $\text{DSP}_{h,r}(\bar{\boldsymbol{x}}^m, \bar{\boldsymbol{y}}^m)$ and their associated objective function values, respectively, where $h \in \mathcal{H}, r \in \mathcal{R}$.

The framework of the basic Benders decomposition algorithm is presented in Algorithm EC.2. The algorithm terminates when no additional Benders cuts can be separated and returns the optimal solution for the MP. As the cardinality of any of the extreme point set $\mathbf{P}(\Lambda_{h,r})$ is bounded for any $h \in \mathcal{H}$ and $r \in \mathcal{R}$, the convergence of the algorithm is guaranteed (Benders 1962).

Algorithm EC.2 Benders decomposition.

Initialize: $terminate \leftarrow$ false, $m \leftarrow 1$, $\mathbf{P}^1(\Lambda_{h,r}) \leftarrow \mathbf{P}^0(\Lambda_{h,r})$, $h \in \mathcal{H}, r \in \mathcal{R}$
while $terminate =$ false **do**
  Solve the MP with Benders cuts in $\mathbf{P}^m(\Lambda_{h,r})$ to obtain $\bar{\boldsymbol{x}}^m$, $\bar{\boldsymbol{y}}^m$, and $\bar{\boldsymbol{z}}^m$
  $terminate \leftarrow$ true
  for $h \in \mathcal{H}$ **do**
    for $r \in \mathcal{R}$ **do**
      Solve the dual subproblem $\text{DSP}_{h,r}(\bar{\boldsymbol{x}}^m, \bar{\boldsymbol{y}}^m)$ to obtain $\bar{\boldsymbol{\chi}}^m_{h,r}$ and $\zeta^m_{h,r}$
      if $\bar{z}^m_{h,r} < \zeta^m_{h,r}$ **then**
        $\mathbf{P}^{m+1}(\Lambda_{h,r}) \leftarrow \mathbf{P}^m(\Lambda_{h,r}) \cup \{\bar{\boldsymbol{\chi}}^m_{h,r}\}$
        $terminate \leftarrow$ false
      end if
    end for
  end for
  $m \leftarrow m + 1$
end while

EC.3.2 Algorithm for subproblem elimination

In iteration m, we let $\bar{\boldsymbol{y}}^m$ denote the vector of solution values for the $y_{k,v}$ variables obtained from solving the MP, and let $\bar{\boldsymbol{Y}}^m$ denote the union of solution vectors from all previous iterations, i.e., $\bar{\boldsymbol{Y}}^m = \bigcup_{m'=1}^{m-1}\{\bar{\boldsymbol{y}}^{m'}\}$. Given $\bar{\boldsymbol{y}}^m$ and $\bar{\boldsymbol{Y}}^m$, the elimination test procedure is defined in Algorithm EC.3. In any iteration of the Benders decomposition algorithm, we do not solve any $\text{PSP}_{h,r}$, $\text{DSP}_{h,r}$, or $\text{PO-DSP}_{h,r}$ such that $\mathbb{I}_{h,r} = 0$, $\forall h \in \mathcal{H}$, $r \in \mathcal{R}$.

Algorithm EC.3 Subproblem elimination in iteration m [SE(m)].

Initialize: the validity of subproblem $\text{DSP}_{h,r}$ as $\mathbb{I}_{h,r} \leftarrow 1$, $\forall h \in \mathcal{H}$, $r \in \mathcal{R}$.
for $h \in \mathcal{H}$ **do**
  for $r \in \mathcal{R}$ **do**
    for $\bar{\boldsymbol{y}}' \in \bar{\boldsymbol{Y}}^m$ **do**
      if $\mathcal{V}_{h,r,k}(\bar{\boldsymbol{y}}') = \mathcal{V}_{h,r,k}(\bar{\boldsymbol{y}}^m)$, $\forall k \in \mathcal{K}$ and $\mathcal{V}_{h,r,0}(\bar{\boldsymbol{y}}') = \mathcal{V}_{h,r,0}(\bar{\boldsymbol{y}}^m)$ **then**
        $\mathbb{I}_{h,r} \leftarrow 0$; Break
      end if
    end for
  end for
end for
Return: $\mathbb{I}_{h,r}$, $\forall h \in \mathcal{H}$, $r \in \mathcal{R}$

EC.3.3 Algorithm for Benders cuts separation with subproblem reduction

Algorithm EC.4 depicts the details of separating Benders cuts with the subproblem reduction techniques introduced in Section 5.3. In the algorithm, $\bar{\boldsymbol{x}}^m$, $\bar{\boldsymbol{y}}^m$, and $\bar{\boldsymbol{z}}^m$ represent the MP solutions in iteration m.

Algorithm EC.4 Benders cuts separation with subproblem seduction in iteration m.

/*Subproblem Elimination*/
Call the Subproblem Elimination subroutine SE(m) (Algorithm EC.3) and obtain validity indices $\mathbb{I}_{h,r}$, $\forall h \in \mathcal{H}$, $r \in \mathcal{R}$; Initiate set of vehicle configurations with solvable subproblems on each route $\mathcal{H}_r^1 \leftarrow \{h \in \mathcal{H} | \mathbb{I}_{h,r} = 1\}, \forall r \in \mathcal{R}$
for $r \in \mathcal{R}$ **do**
  /*Static Grouping*/
  Generate set $\mathcal{J}_r$ and create subsets $\mathcal{H}_{r,j} \subseteq \mathcal{H}_r^1$, $\forall j \in \mathcal{J}_r$; Set $\iota_j \leftarrow 1$, $\forall j \in \mathcal{J}_r$ ▷ $\iota_j = 1$ indicates that subproblems in group $j \in \mathcal{J}_r$ need to be solved.
  Generate vector $\bar{\boldsymbol{z}}_r^* = (\bar{z}_{r,j}^* |, j \in \mathcal{J}_r)$, where $\bar{z}_{r,j}^* = \min_{h \in \mathcal{H}_{r,j}} \{\bar{z}_{h,r}^m\}$, $j \in \mathcal{J}_r$ ▷ $\bar{z}_{r,j}^*$ equals the smallest $\bar{z}_{h,r}^m$ value associated with group $j \in \mathcal{J}_r$.
  Generate vector $\boldsymbol{h}^0 = (h_j^0 | j \in \mathcal{J}_r)$, where $h_j^0 = \arg\max_{h \in \mathcal{H}_{r,j}} \{p_h\}$ ▷ h_j^0 is the configuration with the highest default charging speed in group $j \in \mathcal{J}_r$.
  while $\{j \in \mathcal{J}_r | \iota_j = 1\} \neq \varnothing$ **do**
    Find any $j \in \mathcal{J}_r : \iota_j = 1$
    Set $\iota_j \leftarrow 0$
    Solve $\text{PSP}_{h_j^0,r}(\bar{\boldsymbol{x}}^m, \bar{\boldsymbol{y}}^m)$, collect optimal objective function value $\zeta_{h_j^0,r}$ and solution values in $\bar{\boldsymbol{\alpha}}_{h_j^0}$, and $\bar{\boldsymbol{\beta}}_{h_j^0}$.
    if $\zeta_{h_j^0,r} > \bar{z}_{r,j}^*$ **then**
      Solve $\text{PO-DSP}_{h_j^0,r}(\bar{\boldsymbol{x}}^m, \bar{\boldsymbol{y}}^m, \zeta_{h_j^0,r}, \boldsymbol{x}^c, \boldsymbol{y}^c)$; collect the optimal solution $\bar{\boldsymbol{\chi}}_{h_j^0,r}$
      $\mathbf{P}^{m+1}(\Lambda_{h_j^0,r}) \leftarrow \mathbf{P}^m(\Lambda_{h_j^0,r}) \cup \{\bar{\boldsymbol{\chi}}_{h_j^0,r}\}$
      Call subroutine GS(m, r, j, j) (Algorithm EC.5) for separating Benders cuts associated with group j.
    end if
    if $p_{h_j^0} > \max_{v \in \mathcal{V}_r} \sum_{k \in \mathcal{K}} \bar{y}_{k,v} g_k$ and $\alpha_{h_j^0,i} + \beta_{h_j^0,i} < q_{h_0}$ $\forall i \in \mathcal{N}_r$ **then**
      /*Dynamic Grouping*/
      for $j' \in \mathcal{J}_r : \iota_{j'} = 1, q_{h_{j'}^0} \geq q_{h_j^0}, p_{h_{j'}^0} \geq \max_{v \in \mathcal{V}_r} \sum_{k \in \mathcal{K}} \bar{y}_{k,v} g_k$ **do**
        Set $\iota_{j'} \leftarrow 0$
        if $\zeta_{h_j^0,r} > \bar{z}_{r,j'}^*$ **then**
          Call subroutine GS(m, r, j, j') (Algorithm EC.5) for separating Benders cuts associated with group j'.
        end if
      end for
    end if
  end while
end for

EC.4 Instance generation for assessing benefits of electrification

To generate the instances for assessing benefits of electrification, we first examined the 62 instances with random route samples and $\Gamma = 0$ (i.e., without fleet homogeneity requirements) that were solved to optimality by BD3, as shown in Table 4, and observed that out of the 62 instances, the resultant fleets

Algorithm EC.5 Group-based Benders cut separation [$\mathrm{GS}(m, r, j, j')$].

```
for h ∈ H_{r,j'} do
    if ζ_{h_j^0, r} > z̄^m_{h,r} then
        if (p_h > max_{v∈V_r} Σ_{k∈K} ȳ_{k,v} g_k & q_h = q_{h_j^0}) or (ψ̄_{h_j^0, r} = 0 & p_h = p_{h_j^0} & q_h ≥ q_{h_j^0}) then   ▷ Under these conditions, the following Benders cut is valid and generally stronger.
            P^{m+1}(Λ_{h,r}) ← P^m(Λ_{h,r}) ∪ {χ̄_{h_j^0, r}}
        else
            Solve PO-DSP_{h,r}(x̄^m, ȳ^m, ζ_{h_j^0, r}, x^c, y^c) and collect the optimal solution χ̄_{h,r}
            P^{m+1}(Λ_{h,r}) ← P^m(Λ_{h,r}) ∪ {χ̄_{h,r}}
        end if
    end if
end for
```

in 57 instances were homogeneous. For the remaining 5 instances, we compared their solutions to their counterparts with $\Gamma = 1$ and found an average improvement of 0.7% in the objective function value when the fleet homogeneity requirement was removed. Therefore, as mentioned in Section 6.3, only instances with $\Gamma = 1$ (i.e., with fleet homogeneity requirements) were used for assessing the benefits of electrification. Furthermore, for better out-of-sample performance, we designed a data-driven sampling approach for generating route samples, which is detailed below.

EC.4.1 The Data-driven route sampling approach

Let $\mathcal{R}^0$ be the full set of routes for running the vehicles. Drawing on the method proposed by Wang and Jacquillat (2020), we construct the sample set $\mathcal{R} \subseteq \mathcal{R}^0$ by creating mappings between each route in $\mathcal{R}^0$ and the routes in $\mathcal{R}$. To measure the quality of such mappings, we first establish a distance metric between any two routes r_1 and r_2 in $\mathcal{R}^0$. Let Δ_{r_1,r_2} denote the distance between routes r_1 and r_2, where $r_1, r_2 \in \mathcal{R}^0$. The sample set $\mathcal{R}$ is then created by solving a sampling problem designed to minimize the total mapping distance between the routes in $\mathcal{R}^0$ and their corresponding routes in $\mathcal{R}$. This optimization problem is akin to a *p-median* problem, as described by Reese (2006), and can be formulated as a MILP model. We introduce two sets of binary decision variables: ω_r, which equals 1 if and only if route $r \in \mathcal{R}^0$ is included in $\mathcal{R}$; and ϖ_{r_1,r_2}, which equals 1 if and only if route $r_1 \in \mathcal{R}^0$ is mapped to route $r_2 \in \mathcal{R}$. The formulation of the sampling problem is as follows:

$$\min \quad \sum_{r_1 \in \mathcal{R}^0} \sum_{r_2 \in \mathcal{R}^0} \Delta_{r_1,r_2} \varpi_{r_1,r_2} \tag{EC.16a}$$

$$\text{s.t.} \quad \sum_{r \in \mathcal{R}^0} \omega_r = R, \tag{EC.16b}$$

$$\sum_{r_2 \in \mathcal{R}^0} \varpi_{r_1,r_2} = 1 \qquad \forall r_1 \in \mathcal{R}^0, \tag{EC.16c}$$

$$\varpi_{r_1,r_2} \leq \omega_{r_2} \qquad \forall r_1, r_2 \in \mathcal{R}^0, \tag{EC.16d}$$

$$\omega_r \in \{0,1\} \quad \forall r \in \mathcal{R}^0, \tag{EC.16e}$$

$$\varpi_{r_1,r_2} \in \{0,1\} \quad \forall r_1, r_2 \in \mathcal{R}^0 \tag{EC.16f}$$

where R is the desired size of the sample set $\mathcal{R}$. The objective function (EC.16a) aims to minimize the total mapping distance between routes in $\mathcal{R}^0$ and their counterparts in $\mathcal{R}$. Constraints (EC.16b) ensure the sample set $\mathcal{R}$ is of size R. Constraints (EC.16c) and (EC.16d) guarantee that each route in $\mathcal{R}^0$ maps to exactly one route in the sample set $\mathcal{R}$. The final two sets of constraints stipulate the binary nature of the decision variables.

In our implementation, we define the distances as $\Delta_{r_1,r_2} = |\bar{d}_{r_1} - \bar{d}_{r_2}|$, where $\bar{d}_r = \sum_{a \in \mathcal{A}_r} d_a$ for all $r \in \mathcal{R}^0$. While alternative methods for generating the distance metric exist, preliminary experiments have shown that calculating distances based on length differences can yield solutions with high-quality out-of-sample performance. Our empirical results demonstrate that a MILP solver can solve the model with $\mathcal{R}^0$ and any reasonable target sample size R very efficiently. Let $\boldsymbol{\omega}^* = (\omega_r^* | r \in \mathcal{R}^0)$ and $\boldsymbol{\varpi}^* = (\varpi_{r_1,r_2}^* | r_1, r_2 \in \mathcal{R}^0)$ represent the optimal solution derived from solving the model. The sample set $\mathcal{R}$ is then constructed as $\mathcal{R} = \{r \in \mathcal{R}^0 | \omega_r^* = 1\}$, and the weight assigned to each route $r \in \mathcal{R}$, represented by o_r, is calculated as $o_r = Q \sum_{r_1 \in \mathcal{R}^0} \varpi_{r_1,r}^* o_{r_1}^0$, where Q is a scaling factor that represents the number of repetitions of a route within the planning horizon and $o_r^0 = \frac{1}{|\mathcal{R}^0|}$.

References

Ayman Abdelwahed, Pieter L van den Berg, Tobias Brandt, John Collins, and Wolfgang Ketter. Evaluating and optimizing opportunity fast-charging schedules in transit battery electric bus networks. Transportation Science, 54(6):1601–1615, 2020.

Aisha Alabsi, Ammar Hawbani, Xingfu Wang, Ahmed Al-Dubai, Jiankun Hu, Samah Abdel Aziz, Santosh Kumar, Liang Zhao, Alexey V Shvetsov, and Saeed Hamood Alsamhi. Wireless power transfer technologies, applications, and future trends: A review. IEEE Transactions on Sustainable Computing, 10(1): 1–17, 2024.

Yaseen Alwesabi, Zhaocai Liu, Soongeol Kwon, and Yong Wang. A novel integration of scheduling and dynamic wireless charging planning models of battery electric buses. Energy, 230:120806, 2021.

Kun An. Battery electric bus infrastructure planning under demand uncertainty. Transportation Research Part C: Emerging Technologies, 111:572–587, 2020.

Amir H Ansaripoor, Fernando S Oliveira, and Anne Liret. Recursive expected conditional value at risk in the fleet renewal problem with alternative fuel vehicles. Transportation Research Part C: Emerging Technologies, 65:156–171, 2016.

Okan Arslan and Oya Ekin Karaşan. A Benders decomposition approach for the charging station location problem with plug-in hybrid electric vehicles. Transportation Research Part B: Methodological, 93: 670–695, 2016.

I Bakır. Large scale optimization methods for fleet management in long-haul transportation networks. PhD thesis, Georgia Institute of Technology, GA, 2017.

J-F Benders. Partitioning procedures for solving mixed-variables programming problems. Numerische Mathematik, 4:238–252, 1962.

Quentin Botton, Bernard Fortz, Luis Gouveia, and Michael Poss. Benders decomposition for the hop-constrained survivable network design problem. INFORMS Journal on Computing, 25(1):13–26, 2013.

Stephen P Boyd and Lieven Vandenberghe. Convex Optimization. Cambridge University Press, 2004.

Alex Crawford. Opportunity charging: Knowing when it works. https://www.route-one.net/operators/opportunity-charging-finding-when-it-works/, 2020. Accessed February 7, 2026.

Carlo Cunanan, Manh-Kien Tran, Youngwoo Lee, Shinghei Kwok, Vincent Leung, and Michael Fowler. A review of heavy-duty vehicle powertrain technologies: Diesel engine vehicles, battery electric vehicles, and hydrogen fuel cell electric vehicles. Clean Technologies, 3(2):474–489, 2021.

Miquel Estrada, Josep Mensión, Miquel Salicrú, and Hugo Badia. Charging operations in battery electric bus systems considering fleet size variability along the service. Transportation Research Part C: Emerging Technologies, 138:103609, 2022.

Pranav Gairola and N Nezamuddin. Optimization framework for integrated battery electric bus planning and charging scheduling. Transportation Research Part D: Transport and Environment, 118:103697, 2023.

Yi He, Zhaocai Liu, and Ziqi Song. Optimal charging scheduling and management for a fast-charging battery electric bus system. Transportation Research Part E: Logistics and Transportation Review, 142:102056, 2020.

Yi He, Zhaocai Liu, Yiming Zhang, and Ziqi Song. Time-dependent electric bus and charging station deployment problem. Energy, 282:128227, 2023.

Michael Horn, Jennifer MacLeod, Meinan Liu, Jeremy Webb, and Nunzio Motta. Supercapacitors: A new source of power for electric cars? Economic Analysis and Policy, 61:93–103, 2019.

InsideEVs. In 2023, Port of Los Angeles will get 500 kW wireless charging system. https://insideevs.com/news/628702/port-los-angeles-500kw-wireless-charging/, 2022. Accessed February 7, 2026.

International Energy Agency. Global EV Outlook 2024: Moving towards increased affordability. Technical report, International Energy Agency, France, 2024. Accessed February 7, 2026.

Young Dae Ko and Young Jae Jang. The optimal system design of the online electric vehicle utilizing wireless power transmission technology. IEEE Transactions on Intelligent Transportation Systems, 14(3):1255–1265, 2013.

Nicholas D Kullman, Aurelien Froger, Jorge E Mendoza, and Justin C Goodson. frvcpy: An open-source solver for the fixed route vehicle charging problem. INFORMS Journal on Computing, 33(4):1277–1283, 2021.

Charly Robinson La Rocca and Jean-François Cordeau. Heuristics for electric taxi fleet management at Teo Taxi. INFOR: Information Systems and Operational Research, 57(4):642–666, 2019.

Wenlong Li, Yi He, Songhua Hu, Zhengbing He, and Carlo Ratti. Planning dynamic wireless charging infrastructure for battery electric bus systems with the joint optimization of charging scheduling. Transportation Research Part C: Emerging Technologies, 159:104469, 2024.

Xiangda Li, Yun Peng, Yanyan Guo, Wenyuan Wang, and Xiangqun Song. An integrated simulation and AHP-entropy-based NR-TOPSIS method for automated container terminal layout planning. Expert Systems with Applications, 225:120197, 2023.

Zhaocai Liu, Ziqi Song, and Yi He. Planning of fast-charging stations for a battery electric bus system under energy consumption uncertainty. Transportation Research Record, 2672(8):96–107, 2018.

Thomas L Magnanti and Richard T Wong. Accelerating Benders decomposition: Algorithmic enhancement and model selection criteria. Operations Research, 29(3):464–484, 1981.

Sina Moghadasi, Yanxiang Long, Luo Jiang, Sandeep Munshi, Gordon McTaggart-Cowan, and Mahdi Shahbakhti. Design and performance analysis of hybrid electric class 8 heavy-duty regional-haul trucks with a micro-pilot natural gas engine in real-world highway driving conditions. Energy Conversion and Management, 309:118451, 2024.

Charles Morris. The promise of wireless charging: smaller batteries, longer battery life, fewer charging stations. https://chargedevs.com/features/the-promise-of-wireless-charging-smaller-batteries-longer-battery-life-fewer-charging-stations/, 2022. Accessed February 7, 2026.

GF Nemet, S Pachauri, XC Tan, and T Wiedmann. Emissions trends and drivers. Technical report, Intergovernmental Panel on Climate Change, Switzerland, 2022.

Samuel Pelletier, Ola Jabali, Jorge E Mendoza, and Gilbert Laporte. The electric bus fleet transition problem. Transportation Research Part C: Emerging Technologies, 109:174–193, 2019.

Shyam SG Perumal, Richard M Lusby, and Jesper Larsen. Electric bus planning & scheduling: A review of related problems and methodologies. European Journal of Operational Research, 301(2):395–413, 2022.

Josh Reese. Solution methods for the p-median problem: An annotated bibliography. Networks: An International Journal, 48(3):125–142, 2006.

Pierre Vendé, Yannick Kergosien, and Jorge E Mendoza. Optimizing fast charger location for hybrid electric bus transit networks. Transportation Research Part C: Emerging Technologies, 178:105175, 2025.

Kai Wang and Alexandre Jacquillat. A stochastic integer programming approach to air traffic scheduling and operations. Operations Research, 68(5):1375–1402, 2020.

Min Xu, Qiang Meng, and Zhiyuan Liu. Electric vehicle fleet size and trip pricing for one-way carsharing services considering vehicle relocation and personnel assignment. Transportation Research Part B: Methodological, 111:60–82, 2018.

Daniel Yamín, Guy Desaulniers, and Jorge E Mendoza. The electric vehicle routing and overnight charging scheduling problem on a multigraph. INFORMS Journal on Computing, 37(4):808–830, 2025.

Le Zhang, Wenyan Guo, Yadong Wang, Qiaolin Hu, and Yu Han. Optimal charger deployment for electric buses: Incorporating en-route charging and battery management. Transportation Research Part D: Transport and Environment, 140:104603, 2025.

Hengbing Zhao, Andrew Burke, and Marshall Miller. Analysis of class 8 truck technologies for their fuel savings and economics. Transportation Research Part D: Transport and Environment, 23:55–63, 2013.